# Global Transcriptome Profile of the Developmental Principles of in Vitro iPSC-to-Motor Neuron Differentiation

**Emilia Solomon**
LANL
**Katie Davis-Anderson**
LANL
**Blake Hovde**
LANL
**Sofiya N Micheva-Viteva** ( sviteva@lanl.gov )
Los Alamos National Laboratory Bioscience Division https://orcid.org/0000-0002-2693-4333
**Jennifer Foster Harris**
LANL: Los Alamos National Laboratory
**Scott Nikolas Twary**
LANL: Los Alamos National Laboratory
**Rashi Iyer**
LANL: Los Alamos National Laboratory

**Research article**

**Keywords:** iPSCs, motor neurons, stem cell reprogramming, transcriptomics, neuronal development, in vitro neuronal networks

**Posted Date:** November 19th, 2020

**DOI:** https://doi.org/10.21203/rs.3.rs-108453/v1



**Version of Record:** A version of this preprint was published on February 18th, 2021. See the published version at https://doi.org/10.1186/s12860-021-00343-z.

# Global Transcriptome Profile of the Developmental Principles of *in vitro* iPSC-to-Motor Neuron Differentiation

**Emilia Solomon[1†], Katie Davis-Anderson[1†], Blake Hovde[1], Sofiya Micheva-Viteva[1*], Jennifer Foster Harris[1], Scott Twary[1], and Rashi Iyer[2*]**

[1] Los Alamos National Laboratory, Bioscience Division, Los Alamos, NM, USA

[2] Los Alamos National Laboratory, Analytics, Intelligence, and Technology Division, Los Alamos, NM, USA

[†] Contributed equally

*** Correspondence:**

Rashi Iyer; Sofiya Micheva-Viteva

Rashi@lanl.gov; Sviteva@lanl.gov

**Abstract**

**Background**: Human induced pluripotent stem cells (iPSC) have opened new avenues for regenerative medicine. Consequently, iPSC-derived motor neurons have emerged as potentially viable therapies for spinal cord injuries and neurodegenerative disorders including Amyotrophic Lateral Sclerosis. However, direct clinical application of iPSC bears in itself the risk of tumorigenesis and other unforeseeable genetic or epigenetic abnormalities.

**Results**: Employing RNA-seq technology, we identified and characterized gene regulatory networks triggered by chemical reprogramming of iPSC into motor neurons. We present meta-transcriptome signatures of 5 cell types: iPSCs, neural stem cells, motor neuron progenitors, early motor neurons, and mature motor neurons. In strict response to the chemical stimuli, along the MN differentiation axis we observed temporal downregulation of tumor growth factor-β signaling pathway and consistent activation of sonic hedgehog, Wnt/β-catenin, and Notch signaling. Together with gene networks defining neuronal differentiation (neurogenin 2, microtubule-associated protein 2, Pax6, and neuropilin-1), we observed steady accumulation of motor neuron-specific regulatory genes, including Islet-1 and homeobox protein HB9. Interestingly, transcriptome profiling of the differentiation process showed that $Ca^{2+}$ signaling through cAMP and LPC was downregulated during the conversion of the iPSC to neural stem cells and key regulatory gene activity of the pathway remained inhibited until later stages of motor neuron formation. Pathways shaping the neuronal development and function were well -represented in the early motor neuron cells including, neuroactive ligand-receptor interactions, axon guidance, and the cholinergic synapse formation. A notable hallmark of our *in vitro* motor neuron maturation in monoculture was the activation of genes encoding G-coupled muscarinic acetylcholine receptors and downregulation of the ionotropic nicotinic acetylcholine receptors expression. We observed the formation of functional neuronal networks as spontaneous oscillations in the extracellular action potentials recorded on multi-electrode array chip after 20 days of differentiation.

**Conclusions**: Detailed transcriptome profile of each developmental step from iPSC to motor neuron driven by chemical induction provides the guidelines to novel therapeutic approaches in the re-construction efforts of muscle innervation.

**Keywords**: iPSCs, motor neurons, stem cell reprogramming, transcriptomics, neuronal development, *in vitro* neuronal networks.

## Background

Human neuronal tissue lacks regenerative capacity, leaving few treatments available following neuronal injury or neurodegeneration. In the past decade, an interest in direct neuronal reprogramming of stem cells into motor neurons (MNs) has emerged as a solution to generate human neuronal tissue for therapeutic applications. MNs form synapses to potentiate electrical signals from the CNS into peripheral tissues. They play a critical role in the formation of neuromuscular junctions (NMJs), where MN axons terminate on muscle fibers and neurotransmitters are released to trigger muscle contractions. NMJs are cholinergic synapses, where the neurotransmitter acetylcholine (ACh) is released from the presynaptic MN terminal for uptake by postsynaptic ACh receptors on the target muscle cell (1). This critical function is disrupted in neurodegenerative motor neurons diseases like as Amyotrophic Lateral Sclerosis (ALS) .

Several *in vitro* protocols have been developed to convert progenitor cells, such as human inducible pluripotent stem cells (iPSCs), into MNs (2-4). There are still challenges limiting clinical application of these iPSC-derived MNs. For example, the generation of physiologically active neurons requires a lengthy cell maturation period and often results in a heterogeneous population of neuronal subtypes (5). Protocol reproducibility can also vary as different cell lineages have unique maturation and functional properties. To address these challenges, we present a 28-day transcriptome study coupled with functional assays. Our main objective was to resolve the

underlying mechanisms driving MN differentiation. The results from this study can guide experimental strategies to obtain populations highly enriched with the desired MN subtype.

Here, we followed an established protocol (6) to differentiate iPSCs into MNs using chemically defined media conditions. Efficient neural conversion is based on mimicking *in vivo* neurogenesis where extrinsic and intrinsic signals are introduced in culture, yielding a relatively pure MN population (7, 8). During neuronal differentiation, there are cascading effects as signaling pathways activate transcription factors to upregulate expression of MN specific genes. Neural induction of iPSCs is driven by simultaneous inhibition of tumor growth factor-β (TGFβ), activin, Nodal, and bone morphogenic protein (BMP) signaling. Similar to processes that occur during early development, inhibition of those signaling pathways promotes differentiation along the neuronal lineage primarily through inhibition of pluripotency and blocking alternative lineage differentiation. Several other pathways, including the Wnt signaling pathway, regulate neuronal differentiation. The protocol implemented in this study included three core chemical compounds to inhibit TGFβ and BMP signaling pathways and simultaneously activate Wnt signaling. Following neural induction of iPSCs, neuronal progenitor cells were patterned with all-trans retinoic acid (RA), to promote caudal (spinal cord) identity, and ventralization was promoted by activation of Shh signaling with Purmorphamine. Finally, synchronization of the maturation process, through elimination of dividing cells, was aided by inhibition of the Notch signaling pathway resulting in mature MNs.

Genome-wide transcriptome studies provide in-depth knowledge of regulatory pathways that shape cellular morphology and function. Such information is crucial for the design of novel neuron regenerative therapies and cell-based drug discovery platforms. Previous studies based on single cell transcriptomics of Amyotrophic Lateral Sclerosis (ALS) patient-derived iPSCs discovered the

underlying mechanisms of disease pathology (9) and the regulatory dynamics of MN differentiation (10). Others have investigated the iPSC-derived MN axonal transcriptome and found key regulatory pathways presenting potential drug targets for treatment of genetic disorders (11). A detailed transcriptomics study by Burke *et al.* proposed an influence of the genetic background of the iPSC donors on each pivotal step of iPSC-initiated corticogenesis (12). Further, single cell RNA-seq analysis of iPSC-derived spinal MN demonstrated that *in vitro* differentiation does not produce a homogeneous MN population (8).

Here we performed a comprehensive transcriptomic analysis of *in vitro* iPSCs-derived MNs to characterize the key principles of MN development by analyzing bulk transcriptome data from five crucial time points of MN neurogenesis: iPSCs (D0), NSCs (D7), post-mitotic MNP cells (D13), eMNs (D18), and mature MNs (D28). We interrogated the transcriptomic signatures using next-generation RNA-sequencing (RNA-Seq) technology and performed *in situ* validation of key pluripotency and MN specific biomarker expression. Additionally, we characterized the functionality of iPSC-derived MNs via electrophysiological analysis of neuronal network connectivity. Our results corroborate transcriptomic profiles previously identified in the astrocyte-to-neuron transformation process (3); specifically, upregulation of Shh and Wnt signaling pathways. We observed altered gene expression of TGFβ signaling components during the early stages of iPSC conversion into neural stem cell (NSC) in response to chemical inhibition. However, we detected an upregulation of positive TFGβ regulators in the subsequent steps of neurogenesis.

By applying a LANL-developed Ontology Pathway Analysis software (OPaver) we found that calcium ($Ca^{2+}$) signaling through cyclic adenosine monophosphate (cAMP) and LPC is downregulated during the conversion of the iPSC to NSC and remains silenced until the final stage

of MN maturation when the regulatory pathway becomes a driving force for the neuronal synaptic activity. Another key finding is that during the *in vitro* development of MN in 2D monocultures, ionotropic nAChR are expressed in the early MN stage and are subsequently replaced by the G protein coupled receptors (GPCR) -type muscarinic AChR in mature MN, probably due to lack of metabolic stimuli that are naturally released by the muscle tissue *in vivo*. While our findings provide unique insights into the temporal mechanism of iPSC-derived MNs they also indicate the advantages of using a co-culture system, of MN and muscle, to enable the development of physiologically relevant MNs types akin to that obtained *in vivo*.

## Results

### *A four-step process of iPSC differentiation into MNs*

The initiating step for iPSC differentiation to neuronal stem cells (NSC) is driven by inhibition of TGFβ, activin, nodal, and BMP signaling pathways while simultaneously activating the Wnt signaling pathway to sustain cell proliferation. Therefore, to convert undifferentiated iPSCs into a NSC lineage the culture media was supplemented with SB431542 (SB) and DMH-1, inhibitors of activin receptor-like kinases (ALK4, ALK5, ALK7, and BMP), and CHIR99021 (CHIR), a Wnt pathway activator. MNPs and early motor neurons (eMNs) were patterned through activation of the Shh pathway by Purmorphamine (Pur). The final step of MN maturation and specification was aided by a Notch signaling pathway inhibitor, Compound E (CpdE), to synchronize the maturation process through the elimination of dividing cells. Neurotrophic and growth factors were supplemented to facilitate neuronal growth and maturation (Fig. 1A).

Within a 13-day period, we observed changes in cell morphology, including a gradual reduction in the cell soma and multiple extensions of thin neurites upon iPSCs conversion into MNPs.

Furthermore, we monitored protein accumulation of tissue-specific markers via immunohistochemistry staining (Fig. 1B). Consistent with the morphological features exemplified by high nuclear-to-cytoplasmic ratio and compact multilayer colonies (13), the undifferentiated iPSCs expressed a key pluripotency marker, Oct4 (Fig. 1B; D0). We noted the formation of NSCs at D7 by the disappearance of Oct4 and the accumulation of Nestin and Pax6. Nestin, implicated in cell division and radial axon growth (14, 15), was downregulated by D13 which coincided with increased expression of the pan-neuronal filament protein class III β-Tubulin (βIII-Tub). Cells entered the MNP developmental stage on D13 and transformed to eMNs on D18 when both Nestin and Pax6 expression was significantly downregulated (Fig. 1B). Finally, we detected mature MNs featuring high levels of the structural proteins, βIII-Tub and microtubule-associated protein 2 (MAP2); and increased accumulation of MN specific markers: MN homeobox protein (HB9), choline acetyltransferase (ChAT), and the synaptic vesicles protein (Synaptophysin) (Fig. 1C). HB9 is an essential transcription factor and early marker of cholinergic neurons (16) and ChAT is an enzyme required for the synthesis of the neurotransmitter acetylcholine (ACh). The changes in morphology were pronounced as dendrites extended and expressed MAP2, a neuron-specific cytoskeletal protein critical for successful projection of dendrites (17, 18).

*MNs form functional network connections*

MN activity was characterized by multi-electrode array (MEA) recordings of cellular electrophysiological responses. This non-invasive method allows for repetitive recordings of spontaneous electrical firings at various times during neuronal differentiation. Spontaneous oscillations in extracellular AP were recorded after day 20 of neuronal differentiation, and the AP frequency increased the longer the cells differentiated on the MEA (Fig. 2A). By day 31 (D31) the firing patterns became more organized in highly synchronous bursts of network activity. The AP

spike rate increased as differentiation progressed (Fig. 2B). The increase in the number of bursts, and percentage of spikes in bursts, signified successful formation of synaptic connections with synchronized AP firings (Fig. 2C).

*Unbiased transcriptome analysis of chemically stimulated iPSC differentiation into MNs*

We performed whole-genome transcriptome analysis on RNA-Seq platform to explore gene regulatory pathways. Three independent biological replicates were collected and analyzed at each stage: iPSCs, NSCs, MNPs, eMNs, and MNs. The principal component analysis (PCA) of global transcriptome data revealed tight clustering of all replicates, indicating high reproducibility of gene expression profiles for each stage of development. Differentiation timepoints showed distinct genetic programs, as evidenced by the PCA variances (Fig. 3A). Applying pair-wise analyses, we further compared the differential gene expression profiles between cell populations at various developmental stages. The number of differentially expressed genes (DEGs) increased at each timepoint throughout the differentiation process when compared to D0, illustrating the steady transformation of iPSCs into MNs driven by chemical stimuli (Fig. 3B). The greatest number of DEGs occurred upon the initial culturing of iPSCs in neural differentiation media supplemented with an inhibitor of TGFβ signaling pathway and a Wnt pathway agonist (Fig. 3C; D7-D0).

We analyzed RNA-Seq data with the NCBI Database for Annotation, Visualization and Integrated Discovery (DAVID) v6.8 (19) which categorized DEGs between D0 and D28 by gene ontology (GO) terms (Fig. 4A). Of the upregulated genes, 2,118 were recognized by DAVID and 1683 (79.5%) mapped to specific GO terms consistent with a shift from undifferentiated mitotic cells (iPSC) to differentiated cells of the neuronal lineage. The upregulated DEGs were associated with GO terms specific to neuronal development: 98 genes were related to dendrites; 144 genes were

involved in cell junctions, 68 genes were associated with axon formation, and 61 genes were involved in the postsynaptic membrane. Of the genes downregulated on D28 versus D0, DAVID recognized 1361 genes of which 1234 (90.7%) mapped to a specific GO. The downregulated genes were characteristic of cells undergoing active DNA replication, transcription, and translation associated with nucleoplasm (440 genes), nucleolus (170 genes), nucleus (556), and cytosol (354) GO terms (Fig. 4A).

LANL-developed OPaver (20) identified 12 gene signaling pathways that were significantly ($p<0.05$) altered during iPSC conversion to MNs (Fig. 4B). The top 5 KEGG pathways represented genes involved in cancer regulation, axon guidance, calcium signaling, PI3K-Akt signaling, and MAPK-signaling pathways (Fig. 4B). The OPaver analysis further highlighted the critical role of membrane proteins in cell-to-cell interactions for neuronal development; specifically, neuroactive ligand-receptor interactions and the development of cholinergic synapses.

By focusing our analysis on cellular development pathways, we found significantly altered gene expression profiles of genes involved in TGFβ, Notch, and Shh signaling pathways (Figure 5). Contrary to our expectations, 7 days after chemical inhibition of TGFβ, we observed a significant downregulation of genes acting as negative regulators of TGFβ signal transduction: *PMEPA1* and *TGIF1*, repressors of SMAD2 function, and *SKIL* the nuclear repressor of TGFβ-responsive genes (21). At the same time, a gene positively regulated by TGFβ signaling, *JUNB*/*AP1*, was upregulated (Fig. 5A). These data indicate there was a transient inhibition (lasting less than 7 days) of the TGFβ signaling pathway, when small molecules were present in the culture media to target ALK receptor kinases. In the Notch signaling pathways, we observed a downregulation of *Hes1*, *NOTCH2*, and *PRKCA* after NSCs conversion into MNPs (Fig. 5B; D13). Interestingly, gene expression of *Hes5* and *JAG1* was upregulated until D18 when cells entered the eMN

developmental stage. The final MN maturation phase required the addition of CpdE, a Notch signaling pathway inhibitor (22), along with growth factors: insulin-like growth factor 1 (IGF-1), brain-derived neurotrophic factor (BDNF), and ciliary neurotrophic factor (CNTF). Our results indicated that downregulation of Notch regulators *JAG1* and *Hes5* gene expression was required for the maturation of MNs (Fig. 5B; D28). Shh signaling is essential for patterning and specification of neuronal cells. Significant activation of a key Shh receptor gene, *PTCH1*, was observed at D7 prior to the addition of Pur, and remained upregulated throughout the differentiation process but decreased in MNs (D28), indicating that this gene may act as a positive regulator of cell division in human neuronal cells. In contrast, *ARHGAP36* and *CRMP1* genes were downregulated upon transition of iPSCs to NSCs (D7) and responded to Pur with gradual stimulation of gene expression in MNs at D18-28 (Fig. 5C).

*Validation of RNA-Seq data via RT-qPCR*

Applying RT-qPCR we further validated a subset of key gene markers of pluripotency, NSCs, MNPs, and MNs which were found to be differentially expressed by RNA-Seq profiling. Both methods detected the rapid decrease of pluripotency marker *Oct4* by D7 and increase of *Nestin*, *Pax6*, and *NgN2* expression reaching peak levels at D13 (Fig. 6A-D). Markers of MN specification (*Isl1*, *HB9*, *MAP2*, and *ChAT*) increased throughout the course of neuronal maturation (Fig. 6E-F, H). *ChAT* expression levels gradually increased throughout the differentiation process from NSCs to MNs (Fig. 6H). Collectively, quantitative analysis of gene expression via RNA-Seq closely correlated with RT-qPCR data showing dynamics of gene activities typical for the conversion of pluripotent cells to MNs. We observed transient activation of *Nestin*, a key regulator of cytoskeletal dynamics and cell division in NSC, and stable expression of pan-neuronal markers *Pax6*, *NgN2*, and *MAP2*. Our data indicated there was gradual accumulation of gene transcripts

responsible for the synthesis of neurotransmitter, *ChAT*, and transcription factors, *Isl1* and *HB9*, whose concerted actions shape the phenotype and physiological activity of MNs.

*Cell signaling pathways driving iPSC conversion to MNs*

The GO analysis, conducted by OPaver, identified 12 pathways that included a high number of DEGs as iPSCs were differentiated into MNs. We further investigated the DEG pattern of individual genes in the pathways listed below which had a critical role in shaping neuronal development and function (Tables 1-5). In each description below, 'upregulated' and 'downregulated' gene expression refers to a significance of $p < 0.05$ and $\log_2$ fold change $\geq 2$ between sampling timepoints.

*MAPK-signaling pathway*

MAPK-signaling (Table 1) has an important role in mediating neuronal differentiation and survival (23). Consistent with our expectations, the transition from iPSCs to NSCs was guided by inhibition of signal transduction pathways supporting self-renewal and activation of genes regulating neuron-specific development pathways. Gene expression of Neurotrophic Tyrosine Kinase Receptor type 2, *NTRK2*, was prominently upregulated at D7 when the NSC population was established, while a subset of genes encoding for γ-subunits of voltage-dependent calcium-channels (Cavs) were dramatically downregulated (*CACNG5*, *CACNG7*, and *CACNG8*), along with *MYC*, Ras guanyl-releasing protein 2 (*RASGRP2*), and *GNG12*. Gene groups encoding the auxiliary subunits of high-voltage activated (HVA) Cavs were upregulated during the early stages of neuronal development (24): *CACNB3* (induced 4-fold at D7) and *CACNA2D3* (16-fold activation at D7-D13). The late stage of MN formation (D18-D28) was marked by upregulation of *CACNA1E* and *CACNG2*. Several gene groups encoding auxiliary subunits of low-voltage activated (LVA) Cavs (*CACNG5*

and *CACNG8*), were initially downregulated in NSC and later upregulated during the MN maturation stage (D18-D28). Accumulation of Cavs gene transcripts throughout the MN differentiation process is consistent with the increased excitability of neuronal cells (Fig. 2).

Other key components of MAPK-signaling showed oscillatory patterns of gene expression throughout MN formation and maturation. Gene transcripts of *KIT* and its ligand, *KITLG*, which function in stem cell maintenance, were upregulated in NSCs (D7) and downregulated during the transition from MNP to eMN (D13-D18). *KITLG* transcription was again upregulated in MNs (D18-28). KIT signaling promotes cell survival through the activation of PIK3, PLC, and AKT1 pathways and we detected upregulation of *KITLG* gene expression in MNs which may be a response to the addition of IGF-1 in the culture media. Upregulation of various genes regulating cell survival and proliferation in the post-mitotic MN, such as *KDR*, *PTPRR*, *PTPN5*, and *PRKCB*, further exemplifies the MN response to IGF-1 pro-survival stimulus.

*Calcium ($Ca^{2+}$) signaling pathway*

$Ca^{2+}$-signaling (Table 2) is a critical component of synaptic activity and neuronal function (25). Our RNA-Seq data indicated the conversion of iPSCs into NSCs is marked by a significant downregulation of a gene encoding for a serotonin-specific GPCR, 5-hydroxytryptamine receptor 7 (*HTR7*). In addition, adenylate cyclase 2 (*ADCY2*) was also downregulated at this time and is known to act immediately downstream of HTRs. Together, the downregulation of *HTR7* and *ADCY2* indicates a functional silencing of the cAMP-dependent signaling pathway. Furthermore, multiple genes involved in the activation of $Ca^{2+}$ signaling were downregulated: GPCR subunit alpha-14 (*GNA14*), an activator of phospholipase C (LPC); two gene groups encoding inositol 1,4,5-triphosphate receptors (*ITPR2* and *ITPR3*); and ryanodine receptor 2 (*RYR2*). (Fig.5D) One

GPCR from the chemokine family, *CXCR4*, involved in the cytosolic $Ca^{2+}$ mobilization and cell migration, was also markedly upregulated (16-fold) during the transition into NSCs.

A hallmark of the NSC to MNP transition was the accumulation of receptor tyrosine-protein kinase erB-4 (*ERBB4*) transcripts. ERBB4 is activated by epidermal growth factor proteins, neuregulins2/3, to shape the development of neuronal cells through activation of MAPK3/ERK (26, 27). *ERBB4* expression was upregulated by 18-fold in D7-D13, followed by upregulation of *CACNA1B*, *CACNA1E*, *GRIN2A* and *P2RX3* (D13-D18). Formation of eMNs (D13-D18) coincided with upregulated gene expression of HVA N- and R-type (*CACNA1B* and *CACNA1E*) voltage-dependent $Ca^{2+}$ channels, glutamate ionotropic receptor (*GRIN2A*), and the ligand-gated ion channel responsible for peripheral pain responses, *P2RX3*. These gene expression profiles indicate the selective pressure of chemical stimuli lead to the formation of eMNs with characteristics of the sympathetic nerve system (28).

In the final stage of MN maturation (D18-D28), we observed upregulation of gene groups activating $Ca^{2+}$ signaling through the cAMP-dependent pathway: *HTR7* and *ADCY2*. We also detected upregulated expression of the intracellular $Ca^{2+}$ ryanodine receptor 2 (*RYR2*), signifying cell readiness to release $Ca^{2+}$ from the sarcoplasmic reticulum in response to adrenergic (sympathetic) stimulation (Fig.5D). This finding was consistent with the upregulation of *ADRA1A*, which encodes the adrenergic receptor alpha subunit 1α. Furthermore, gene activation of both ionotropic (*GRIN1* and *GRIN2D*) and metabotropic (*GRM1*) glutamate receptors, together with the upregulation of neuromedin-K receptor (*TACR3*), accentuated the role of the IP3-$Ca^{2+}$ second messenger system to activate ERK1/2 as well as classical PKC signaling pathways (29-31). We also detected higher levels of *PRKCB* gene transcripts in MNs compared to eMNs (Table 2).

Interestingly, G-coupled muscarinic acetylcholine receptors (mAChRs) were upregulated in mature MNs (D28). Genes encoding for excitatory (*CHRM3*) and inhibitory (*CHRM2*) mAChRs were specifically activated in late stage MN maturation (Table 2, D18-D28). The excitatory mAChRs stimulate PLC, triggering IP3 and diacylglycerol signaling pathways. Since mAChRs are present on parasympathetic neurons (32), our data suggest that the iPSC-induced MNs bear the excitatory characteristics of parasympathetic neurons.

*Neuroactive ligand-receptor interactions*

The majority of neuronal receptors are GPCRs and they function to regulate signal transduction pathways and shape cellular physiological responses. Our genome wide transcriptome analysis revealed that iPSC-induced MNs differentiation is marked by the expression of neuroactive receptors which are responsive to glutamate, ACh, and catecholamines, orexin, and prostaglandins (Table 3).

During the first step of iPSC commitment to a neuronal lineage, multiple glutamate receptors were altered, notably, gene expression levels of two ionotropic glutamate receptors were upregulated in the NSCs, *GRIA1* and *GRIK1*, while their paralog genes, *GRIA4* and *GRIK4*, were downregulated. This suggests a specific requirement for type 1 ionotropic glutamate receptors early in neuronal development. Neuromedin and apelin receptors (*NMUR2* and *APLNR*) were upregulated in NSCs, as well as GPCR response to sphingosine-1-phosphate signaling receptor (*S1PR1*), suggesting changes in cytoskeleton dynamics and mitosis (33). Genes encoding for nicotinic acetylcholine receptors (nAChR) and cannabinoid receptors (*CNR1*and *CHRNB4*) were upregulated during the conversion of NSCs into MNPs and remained activated until eMNs were formed.

Formation of eMNs was marked by reactivation of genes encoding glutamate receptors which were downregulated at the NSC stage. Gene activity of various ionotropic glutamate receptors peaked when eMNs became mature MNs (D18-D28). Activation of genes regulating the synthesis of various neurotransmitters defined the transition from eMNs to MNs. The transcript levels of the neuropeptide *tachykinin*, and its receptor (*TACR3*), were upregulated in MNs. In spinal neurons, tachykinins evoke synthesis and release of ACh, histamine, catecholamines, and GABA. We also detected differential expression of the somatostatin receptor (*SSTR1*) indicating that the mature MN population can secrete neurotransmitters (34). The glucocorticoid receptor (*NR3C1*) was upregulated in MNPs and MNs and two new classes of neuroactive receptors were upregulated in the last stage of MN maturation: hypocretin/orexin (*HCRTR2*) and prostaglandin E receptor 4 (*PTGER4*). Our transcriptomic data indicate that the replacement of ionotropic nAChR (*CHRNA3*) and dopamine receptor (*DRD2*) expression with adrenergic receptor (*ADRA1A*) and mAChRs (*CHRM2* and *CHRM3*) marked the formation of mature MNs. The controversial activation of mAChRs and genes encoding excitatory neurotransmitters, including glutamate and catecholamines (ADRA1A), could stem from the formation of a heterogeneous population consisting of parasympathetic and sympathetic MNs.

*Axon guidance and cholinergic synapse*

Pathways regulating axon guidance and synapse development were upregulated during iPSC-to-MN differentiation (Tables 4 and 5, respectively). These functions are critical for neuronal development, maintenance, and repair mechanisms.

We found netrin-G1 (*NTNG1*) to be initially downregulated as iPSCs transitioned into NSC, but then upregulated in eMNs and MNs from D13-28. Deleted in colorectal carcinoma *(DCC*) was

also significantly upregulated as iPSCs transition through NSCs to become MNPs, indicating its critical role in prompting axon extension. *SLIT1* was upregulated at D7 and both *SLIT1* and *SLIT2* were upregulated as the NSCs became MNPs (D7-D13). HB9 tightly regulates Robo2 expression to regulate motor axon guidance in ventrally-projecting MNs (35) and we observed *ROBO2* downregulation in NSCs, during which time HB9 transcripts were initially accumulating (Fig. 6G).

*In vivo* as MN axons extend, they have the potential to terminate on a muscle fiber at a cholinergic synapse, the site of ACh neurotransmission. In the pre-synaptic neuron, ACh synthesis is driven by choline O-acetyltransferase (ChAT) and we observed *ChAT* gene expression to be increased in both eMNs and MNs. Expression of ion-channel-coupled nAChR subunits were also significantly altered: *CHRNA3* was regulated in NSCs but downregulated in MNs and *CHRNA4* was upregulated at the eMN stage. In the postsynaptic membrane these receptor components would contribute to neuroactive ligand-receptor interactions as previously described. Gene expression of acetylcholinesterase (*AChE*) was significantly increased late in MNs maturation (D18-D28), which encodes an enzyme responsible for the hydrolysis of ACh into choline and acetic acid, a critical step in ACh recycling in the cholinergic synapse. Membrane transporter solute carrier family 5 member 7 (SLC5A7) is then able to import choline back into a cholinergic neuron for subsequent ACh synthesis. We found gene expression of *SLC5A7* to be increased in both the eMNs and mature MNs.

## Discussion

This comprehensive study documents transcriptomic and morphological changes of iPSCs as they differentiate into motor neurons (MNs) *in vitro*. We performed RNA-Seq meta-transcriptome analysis of human iPSC and the four cell types representing stages of spinal motor neuron

differentiation (NSC, MNP, and eMN) and maturation (MN). The results from our genome-wide transcriptome study revealed basic developmental principles of *in vitro* neurogenesis from iPSC that have not been elucidated by previous studies while confirming the regulatory role of TGFβ, Notch, and Shh signaling pathways in the formation of adult spinal motor neurons. We further corroborated the findings from the next-generation RNA-Seq analysis with RT-qPCR gene expression assays and immunohistochemistry profiles of key pluripotency and MN markers. Applying novel OPaver software we found strict temporal correlation between the formation of functional neuronal network connections on a MEA chip and the expression of genes involved in the regulation of $Ca^{2+}$ signaling. We found that cAMP-regulated $Ca^{2+}$ signaling was inhibited on gene transcript level when iPSC traversed through the neurodevelopmental stages and was reactivated in the final stage (D28) of MN maturation when we were able to detect neuronal synaptic activity via recordings of spontaneous AP firings.

*Inhibition of $Ca^{2+}$ signaling is required for the transition from iPSC to NSC*

Intracellular $Ca^{2+}$ levels, known as calcium transients, regulate neuronal subtype and neurotransmitter specifications (36, 37). Our global transcriptome data showed activation of genes regulating $Ca^{2+}$ entry, specifically voltage-sensitive calcium channels and ionotropic glutamate receptors, not sooner than at the eMN developmental stage (D18 vs D13, Table 1 and Fig. 5D). $Ca^{2+}$ signaling comprises a cascade of molecular interactions and biophysical events, which translate extracellular signals to intracellular responses via increase of cytoplasmic $Ca^{2+}$. This can be activated by neurotransmitters, hormones, and growth factors, chemical and electrical stimuli, causing membrane excitation. Two fundamental mechanisms regulate $Ca^{2+}$entry through protein channels: voltage-dependent $Ca^{2+}$ channels and ligand-gated channels. The latter are highly diverse, non-$Ca^{2+}$-specific, and greatly represented by the family of guanine-binding GPCR (38).

Significant upregulation in differentiated MN of high-voltage activated Cavs genes, such as *CACNB3*, is responsible for tight control on intracellular $Ca^{2+}$ signaling through regulation of calcium ($Ca^{2+}$) entry and direct interaction with phospholipase C-coupled (PLC) and inositol trisphosphate (IP3) receptors (39). Upregulation of *CXCR4* by 16-fold at D0-D7 underlines the importance of intracellular $Ca^{2+}$ signaling inhibition as the neuronal cell lineage commitment process begins. The CXCR4/CXCR7 complex recruits β-arrestin to trigger the canonical GPCR pathway activating ERK1/2, p38, and SAPK, while inhibiting both $Ca^{2+}$ mobilization and cAMP signaling (40). Upregulation of neuromedin and apelin receptors (*NMUR2* and *APLNR*) in NSCs suggest a role for phosphoinositide (PI) signaling pathways that inhibit cAMP production upon $Ca^{2+}$ mobilization and possibly in regulating cytoskeleton dynamics, cell growth, and hormone release (41, 42).

Our findings underline the role of temporal gene regulation of $Ca^{2+}$ signaling in motor neuron development *in vitro*. It has been previously demonstrated that voltage-gated $Ca^{2+}$ influx activated by cAMP is instrumental in the maturation of neuronal progenitor cells into functional neurons (43). The comparative transcriptome study presented here revealed that genes regulating cAMP synthesis (ADCY2), voltage-gated calcium channels (CACNA1B and CACNG5), and the receptor regulating the intracellular $Ca^{2+}$ homeostasis (RYR2) were immediately inhibited upon transition of iPSC into NSC and were re-activated in mature MN. Collectively, our data suggests that inhibition of pathways regulating the $Ca^{2+}$ transients is required for the successful transition from pluripotency to neuronal progenitor cells. Our findings corroborate previous studies that have demonstrated that low cellular excitability is vital for cell migration while increase in the $Ca^{2+}$ transients stops migration and promotes dendrite formation in cortical neurons (44).

*MN specification in vitro is driven by the chemical stimuli in growth media and bare the characteristics of the parasympathetic nervous system*

The transcriptome analysis revealed the underlying molecular changes in differentiation of iPSC to mature MNs. Specifically, we observed that short-term inhibition of TGFβ signaling was sufficient to push iPSCs into NSCs and that continuous activation of Notch and Shh signaling pathways ensured morphogenesis and cell survival throughout the MN differentiation and maturation process. While the majority of changes were characteristic of neuronal development, deeper analysis revealed the involvement of more unexpected genes as well as unique temporal changes. For example, the oscillatory pattern of *SKIL* gene expression throughout the neuronal cell differentiation process suggests a regulatory feed-back loop that balances survival and cell differentiation programs. *PTCH1*, a Shh receptor gene, is consistently and significantly upregulated from D7 to D28 suggesting a role as a positive regulator in neuronal cell division. Binding of Shh to PTCH1 results in the release of the smoothened protein initiating cell proliferation. Upon ligand binding, PTCH1 is trafficked away from the Shh positive regulator, G-coupled receptor SMO, resulting in downstream signal transduction (45). Downregulation of *PTCH1* by D28 supports the possible inhibition of cell proliferation and subsequent differentiation to neurons. *ARHGAP36* and *CRMP1*, both of which are downregulated simultaneously, encode for Rho GTPase activating protein 36 and collapsin response mediator protein 1, are implicated in semaphorin-induced growth cone and axon guidance (46, 47) and may regulate cell division and morphogenesis of MNs.

Applying quantitative gene transcript analysis and immunohistochemistry, we observed that *ChAT*, a marker of mature neurons, was upregulated as soon as iPSC committed to a neuronal lineage (D7). In addition, the well-orchestrated expression of key genes such as *Nestin*, *Pax6*,

417 *NgN2*, *MAP2*, *Isl1* and *HB9* corroborated the phenotypic changes to MNs. The patterns of gene
418 expression reported here are consistent with similar studies using small molecules to drive neuron
419 reprogramming from astrocytes (3) or fibroblasts (48).

420 While Shh drives motor neuron formation over intermediate neurons, there are multiple subtypes
421 of MNs. In the final stage of MN maturation, we observed that genes encoding ionotropic nAChR
422 (*CHRNA3*) and dopamine receptor (*DRD2*) were downregulated while adrenergic receptor
423 (*ADRA1A*) and mAChRs (*CHRM2* and *CHRM3*) gene expression was activated. Since mAChRs
424 are found exclusively on the neurons from the parasympathetic system (49) our data indicates that
425 *in vitro* iPSC-derived MN in monoculture have the characteristics of the parasympathetic neurons
426 of the peripheral nervous system.

427 In addition to the parasympathetic neuron-specific mAChRs gene activation, genes encoding
428 excitatory neurotransmitters specific to the sympathetic neurons, including glutamate and
429 catecholamines (ADRA1A), were significantly upregulated in the population of mature motor
430 neurons. This could stem from the formation of a heterogeneous population consisting of
431 parasympathetic and sympathetic MNs. Previous studies based on single-cell RNA-Seq analysis
432 of iPSC-derived spinal MN have demonstrated that the protocol for *in vitro* differentiation
433 produces a mixed population of MN subtypes with a predominant (58%) sub-population of lateral
434 MNs and several minority sub-populations, including hypaxial motor column (19%) and median
435 motor column (6%) MNs (8).

436 *The neuroactive ligands define electrophysiological activity of in vitro iPSC-derived mature MNs*

437 The electrophysiological activity of mature MN reflects their ability to form functional neuronal
438 network connections. Neuronal precursors and neurons are capable of spontaneous electrical

activity (50), and we observed increased electrical activity as synapses and neural circuits formed. As iPSCs differentiated after plating on the MEAs, dendrite projections formed as axons stretched between neuronal cell bodies. These networks of MNs created numerous synapses to propagate nerve impulses. The MEAs were able to capture spontaneous firings of extracellular action potentials as single spikes of activity early in differentiation which progressed to more frequent firing bursts as the iPSC-derived MNs matured, demonstrating peak activity on D31. While the length and amplitude of an action potential are always the same, an increase in the stimulus caused an increase in the frequency of an action potential indicative of an enhanced response.

MNs are often characterized by their role in forming cholinergic synapses at NMJs. MN axons terminate on muscle fibers and nerve impulses are translated into muscle contractions as the neurotransmitter ACh is released from the presynaptic MN terminal for uptake by postsynaptic ACh receptors on the target muscle cell (1). Understanding the underlying mechanism of cholinergic development provides insights about potential treatments for neurodegenerative diseases and strategies to develop countermeasures to chemical toxicology exposure. AChE inhibitors are used to treat Alzheimer's and Parkinson's diseases (51, 52) and cholinergic agonist treatments have shown to improve memory function (53). Similar strategies have been employed to treat organophosphate-induced neurotoxicity (54, 55). Here we show how culture conditions imprint distinct fates and future efforts to co-culture of MNs with other cell types, such as muscle, may cause different neuronal specification. Surprisingly, we observed the expression of nAChRs typically found on the NMJ to be downregulated in mature MN monocultures while the mAChRs were upregulated.

## Conclusions

This study revealed significant changes to the transcriptome, protein expression, and electrical function as iPSCs differentiated into mature MNs. These results can further be applied to characterize aberrant neuronal functions following neurodegeneration or exposure to chemical toxins. Understanding the underlying molecular and cellular cues involved in MN differentiation of iPSCs has the potential to enable the discovery of novel treatments for neural injuries.

## Methods

*Culturing and differentiating iPSCs:*

Human iPSCs (WTC-11, Coriell Institute) were cultured and maintained on vitronectin (ThermoFisher Scientific) treated culture plates in Essential8 medium (ThermoFisher Scientific). Differentiation of iPSCs into MNs was directed as previously described (6). Briefly, iPSCs were cultured in neural media which consisted of 1:1 DMEM/F12 and Neurobasal medium supplemented with N2, B27, 1x Glutamax and 1x penicillin/streptomycin (all from ThermoFisher Scientific), and 0.1mM ascorbic acid (StemCell Technology). On days 0-6 3μM CHIR99021 (StemCell Technology), 2μM DMH-1 (Tocris) and 2μM SB431542 (StemCell Technology) were added to the neural medium; days 6-12 the same media was used with the addition of 0.1μM RA (StemCell Technology) and 0.5μM Pur (Sigma); days 12-18 cells were maintained with 0.1μM RA and 0.5μM Pur added to the neural media; finally from day 18 on cells were cultured with 0.5μM RA, 0.1μM Pur and 0.1μM CpdE (StemCell Technology), IGF-1, BDNF, and CNTF (all from R&D Systems, 10 ng/ml each).

*RNA extraction:*

Cells were lifted with accutase, pelleted by centrifugation, and stored at -20°C. Total RNA was extracted from cell pellets using RNeasy Mini Kit (Qiagen), following the recommendations of the manufacturer. After DNase digestion by Turbo DNA-free kit (ThermoFisher Scientific), samples were quantified and divided for qPCR and transcriptomic analyses.

*RNA sequencing analysis:*

Extracted and DNase-treated RNA was quantified using the Qubit 4 Fluorometer (ThermoFisher) with the High Sensitivity RNA reagents and Bioanalyzer (Agilent) with RNA 6000 Pico reagents. Ribosomal depletion, DNA conversion, and library preparation was performed on all samples using the Illumina TruSeq Stranded Total RNA kit. 151 base pair reads were sequenced on the Illumina NextSeq. Across fifteen samples (three independent experiments x five time points) the total number of reads generated for each sample ranged from approximately 26 million to 40 million reads. Sequencing data was quality trimmed using FaQCs (56) with a quality score cutoff of Q20. Differential expression analysis was performed using PiReT (57) V 0.3.2 and utilizing DEseq2 (58) default parameters and setting a q-value of 0.05 (false discovery rate metric). The experimental design file (provided in the supplementary material) was used to dictate the replicate sample ID's and sequencing data to be used in the PiReT analysis. Human genome version hg38 was used as the reference genome. KEGG (59, 60) pathway mapping was performed using Omics Pathway Viewer - 'OPaver' (Li, unpublished). Raw RNA-Seq reads were deposited in the NCBI SRA database under the accession numbers SRR11994167- SRR11994181. Metadata for each sample are also accessible under NCBI BioProject PRJNA638768.

*Quantitative reverse transcription PCR (RT-qPCR):*

Three independent experiments were run in duplicate using a 7500 Fast Real-Time PCR System (Applied Biosciences). 50ng of each RNA sample were probed for motor neuron differentiation markers using Taqman RNA-to-CT 1-Step Kit (Applied Bioscience) in a 25µl volume according to the manufacturer's instructions. Taqman probes included NEUROG2 (Hs00935087_g1), ChAT (Hs00758143_m1), Isl1 (Hs01099686_m1), PAX6 (Hs01088114_m1), MAP2 (Hs00258900_m1), Nestin (Hs04187831_g1), Oct4 (Hs00999632_g1), and HB9 (Hs00907365_m1). Two endogenous controls, actin (Hs99999903_m1) and GAPDH (Hs01922876_u1), were analysis by RT-qPCR and no significant differences were observed in their expression levels (data not shown); thus, all data shown are normalized to GAPDH.

*Immunohistochemistry staining:*

Nunc Lab-Tek chamber slides (ThermoFisher Scientific) were coated with vitronectin, seeded, and subsequently fixed with 4% paraformaldehyde, permeabilized with 0.4% Triton X-100, blocked with 3% BSA in PBS for at least 1 hour. Samples were incubated overnight at 4°C with primary antibody solutions (Table 6) diluted in PBS containing Image-iT FX signal enhancer. Cells were washed with PBS three times prior to incubation with NucBlue Fixed Cell Reagent, Image-iT FX signal enhancer, and secondary Alexa-488-, Alexa 555-, or Alexa 647-conjugated antibodies at 37°C for 2 hours (1:1000 dilution, ThermoFisher Scientific and Jackson ImmunoResearch). After three PBS washes, the media chambers were removed from the glass slide, coverslips were mounted using ProLong Diamond Antifade Mountant and cells were examined using fluorescence microscopy (Zeiss Observer Z.1).

Table 6: List of primary antibodies

| Antibody | Species | Dilution | Source |
|---|---|---|---|
| Oct4 | Rabbit | 1:200 | Cell Signaling Technology (Cat# 2750S) |
| Nestin | Rabbit | 1:200 | Abcam (Cat# ab105389) |
| Pax6 | Mouse | 1:50 | Developmental Studies Hybridoma Bank (Ca# Pax6) |
| MAP2 | Mouse | 1:200 | ThermoFisher (Cat# MA5-12823) |
| HB9 / MNX1 | Mouse | 1:50 | Developmental Studies Hybridoma Bank (Cat# 81.5C10) |
| ChAT | Goat | 1:100 | Milipore (Cat#AB144P) |
| beta-III-tubulin | Rabbit | 1:1000 | Abcam (Cat# ab18207) |
| Synaptophysin [SY38] | Mouse | 1:100 | Abcam (Cat# ab8049) |

*Functional analysis of MNs on microelectrode array (MEA):*

Cells were seeded on MEA chips, either in 60MEA200/30iR-Ti arrays or 24-well Plate with PEDOT Electrodes on Glass, 24W300/30G-288 (Multichannel Systems). MEA's were coated with poly-D-lysine and vitronectin. Before recording, the MEA chips were moved to the MEA2100 system (MultiChannel Systems) equipped with temperature control and allowed to equilibrate for 10 minutes before recording. The data were acquired using Multi Channel Experimenter or Multiwell Screen (MultiChannel Systems) at a sampling rate of 20 kHz for 2 min at 37ºC. Data were filtered using Butterworth band pass filter with 200Hz cutoff frequency and threshold of 5 x SD were set to minimize both false-positive and missed detection. The representative electrodes were selected for analysis of mean spike frequency and percentage of spikes in the burst.

*Transcriptome Analysis:*

DAVID Functional Annotation Bioinformatics Microarray Analysis can be accessed at https://david.ncifcrf.gov. The raw transcriptomic data of D0-D28 significant DEGs ($p<0.05$) included 2242 upregulated and 1438 downregulated terms, available in the supplemental material. Each list of homo sapiens genes was independently analyzed by DAVID, to generate an analysis of associated gene ontology (GO) terms.

OPaver (Li, unpublished), is a web-based tool to integrate multiple types (e.g. transcriptomics, proteomics and metabolomics) and time series of data to KEGG biochemical pathways maps. This software analysis tool was developed at Los Alamos National Laboratory. In this case, OPaver was utilized to map significantly differentially expressed genes ($p<0.05$) identified in the DEseq2 analysis performed by PiRet. Differential expression calculation from DEseq2 in Log2 fold change and associated genes (provided in the supplementary material) were used as input for the OPaver software.

**List of abbreviations**

**ACh:** Acetylcholine

**ALS:** Amyotrophic Lateral Sclerosis

**AP:** Action potentials

**BDNF:** Brain-derived neurotrophic factor

**βIII-Tub:** Class III β-Tubulin

**BMP:** Bone morphogenic protein

**cAMP:** cyclic adenosine monophosphate

**Cavs:** Voltage-dependent calcium-channels

**ChAT:** Choline acetyltransferase

**CHIR:** CHIR99021

**CNTF:** Ciliary neurotrophic factor

**CpdE:** Compound E

**D0:** Day 0

**D7:** Day 7

**D13:** Day 13

**D18:** Day 18

**D28:** Day 28

**D31:** Day 31

**DAVID:** Database for Annotation, Visualization and Integrated Discovery

**DEGs:** Differentially expressed genes

**eMNs:** Early Motor Neurons

**GO:** Gene ontology

**GPCR:** G protein-coupled receptors

**HVA:** High-voltage activated

572 **IP3:** Inositol trisphosphate

573 **iPSC:** Induced pluripotent stem cells

574 **IGF-1:** Insulin-like growth factor 1

575 **Isl1:** Islet-1

576 **LVA:** Low-voltage activated

577 **LANL**: Los Alamos National Laboratory

578 **mAChRs:** Muscarinic acetylcholine receptors

579 **MAP2:** Microtubule-associated protein 2

580 **MEA:** Multi-electrode array

581 **MN:** Motor neurons

582 **MNPs:** Motor neuron progenitors

583 **nAChR:** Nicotinic acetylcholine receptor

584 **NMJs:** Neuromuscular junctions

585 **NSCs:** Neural stem cells

586 **OPaver:** Ontology Pathway Analysis software

587 **PCA:** Principal Component Analysis

588 **PLC:** Phospholipase C

589 **Pur:** Purmorphamine

590 **RA:** all-trans retinoic acid

591 **RNA-Seq:** RNA-sequencing

592 **SB:** SB431542

593 **Shh:** Sonic hedgehog

594 **TGFβ:** Tumor growth factor-β

595

596 **Declarations**

597 *Ethics approval and consent to participate* (Not applicable)

598 *Consent for publication* (Not applicable)

599 *Availability of data and materials*

600 The datasets generated for this study can be found in the NCBI SRA database under accession
601 numbers SRR11994167- SRR11994181, NBCI BioProject
602 PRJNA638768, [https://www.ncbi.nlm.nih.gov/bioproject/PRJNA638768] and NCBI
603 BioSamples SAMN15207814-SAMN15207828.

604 *Competing interests*

605 The authors declare that they have no competing interests.

*Funding*

Research presented in this article was supported by the Laboratory Directed Research and Development program of Los Alamos National Laboratory under project number 20190167.

*Authors' contributions*

**ES:** Methodology, Investigation, Visualization, Formal analysis, Writing – review and editing; **KDA:** Writing original draft, Visualization, Formal analysis; **BH:** Formal analysis; **SMV:** Formal analysis, Writing-original draft; **JFH:** Supervision; **ST:** Writing – review and editing, Supervision, and **RI:** Supervision, Writing – review and editing. The final version was approved by all authors.

*Acknowledgements*

We greatly valued helpful discussions with Paul Li and Bin Hu, as well as Arasely Rodriguez's technical assistance.

**References**

1. Legay C, Mei L. Moving forward with the neuromuscular junction. J Neurochem. 2017;142 Suppl 2:59-63.

2. Sances S, Bruijn LI, Chandran S, Eggan K, Ho R, Klim JR, et al. Modeling ALS with motor neurons derived from human induced pluripotent stem cells. Nat Neurosci. 2016;19(4):542-53.

3. Ma NX, Yin JC, Chen G. Transcriptome Analysis of Small Molecule-Mediated Astrocyte-to-Neuron Reprogramming. Front Cell Dev Biol. 2019;7:82.

4. Davis-Dusenbery BN, Williams LA, Klim JR, Eggan K. How to make spinal motor neurons. Development. 2014;141(3):491-501.

5. Amoroso MW, Croft GF, Williams DJ, O'Keeffe S, Carrasco MA, Davis AR, et al. Accelerated high-yield generation of limb-innervating motor neurons from human stem cells. J Neurosci. 2013;33(2):574-86.

6. Du ZW, Chen H, Liu H, Lu J, Qian K, Huang CL, et al. Generation and expansion of highly pure motor neuron progenitors from human pluripotent stem cells. Nat Commun. 2015;6:6626.

7. Petros TJ, Tyson JA, Anderson SA. Pluripotent stem cells for the study of CNS development. Front Mol Neurosci. 2011;4:30.

8. Thiry L, Hamel R, Pluchino S, Durcan T, Stifani S. Characterization of Human iPSC-derived Spinal Motor Neurons by Single-cell RNA Sequencing. Neuroscience. 2020.

9. Namboori SCT, P.; Ames, R.; Garrett, L. O.; Willis, C. R.; Stanton, L. W.; and Bhinge A. Single cell transcriptomics identifies master regulators of dysfunctional pathways in SOD1 ALS motor neurons. bioRxiv. 2019;593129.

10. Sagner A, Gaber ZB, Delile J, Kong JH, Rousso DL, Pearson CA, et al. Olig2 and Hes regulatory dynamics during motor neuron differentiation revealed by single cell transcriptomics. PLoS Biol. 2018;16(2):e2003127.

11. Maciel R, Bis DM, Rebelo AP, Saghira C, Zuchner S, Saporta MA. The human motor neuron axonal transcriptome is enriched for transcripts related to mitochondrial function and microtubule-based axonal transport. Exp Neurol. 2018;307:155-63.

12. Burke EE, Chenoweth JG, Shin JH, Collado-Torres L, Kim SK, Micali N, et al. Dissecting transcriptomic signatures of neuronal differentiation and maturation using iPSCs. Nat Commun. 2020;11(1):462.

13. Courtot AM, Magniez A, Oudrhiri N, Feraud O, Bacci J, Gobbo E, et al. Morphological analysis of human induced pluripotent stem cells during induced differentiation and reverse programming. Biores Open Access. 2014;3(5):206-16.

14. Bott CJ, Johnson CG, Yap CC, Dwyer ND, Litwa KA, Winckler B. Nestin in immature embryonic neurons affects axon growth cone morphology and Semaphorin3a sensitivity. Mol Biol Cell. 2019;30(10):1214-29.

15. Sunabori T, Tokunaga A, Nagai T, Sawamoto K, Okabe M, Miyawaki A, et al. Cell-cycle-specific nestin expression coordinates with morphological changes in embryonic cortical neural progenitors. J Cell Sci. 2008;121(Pt 8):1204-12.

16. Arber S, Han B, Mendelsohn M, Smith M, Jessell TM, Sockanathan S. Requirement for the homeobox gene Hb9 in the consolidation of motor neuron identity. Neuron. 1999;23(4):659-74.

17. Harada A, Teng J, Takei Y, Oguchi K, Hirokawa N. MAP2 is required for dendrite elongation, PKA anchoring in dendrites, and proper PKA signal transduction. J Cell Biol. 2002;158(3):541-9.

18. Soltani MHP, R.; Song, Z.; Sangha, N.; Camacho, F.; Satyamoorthy, K.; Sangueza, O.P.; Setaluri, V. Microtubule-Associated Protein 2, a Marker of Neuronal Differentiation, Induces Mitotic Defects, Inhibits Growth of Melanoma Cells, and Predicts Metastatic Potential of Cutaneous Melanoma. Am J Patho. 2005;166(6):1841-50.

19. Huang D.W.; Sherman BTL, R.A. Systematic and integrative analysis of large gene lists using DAVID Bioinformatics Resources. Nature Protoc. 2009;4(1):44-57.

20. Li PECP. OPaver: Omics Pathway Viewer.

21. Tecalco-Cruz AC, Sosa-Garrocho M, Vazquez-Victorio G, Ortiz-Garcia L, Dominguez-Huttinger E, Macias-Silva M. Transforming growth factor-beta/SMAD Target gene SKIL is negatively regulated by the transcriptional cofactor complex SNON-SMAD4. J Biol Chem. 2012;287(32):26764-76.

22. Huang P, Xiong F, Megason SG, Schier AF. Attenuation of Notch and Hedgehog signaling is required for fate specification in the spinal cord. PLoS Genet. 2012;8(6):e1002762.

23. Fukunaga K, Miyamoto E. Role of MAP kinase in neurons. Mol Neurobiol. 1998;16(1):79-95.

24. Lacinova L. Voltage-dependent calcium channels. Gen Physiol Biophys. 2005;24 Suppl 1:1-78.

25. Brini M, Cali T, Ottolini D, Carafoli E. Neuronal calcium signaling: function and dysfunction. Cell Mol Life Sci. 2014;71(15):2787-814.

26. Tan W, Dean M, Law AJ. Molecular cloning and characterization of the human ErbB4 gene: identification of novel splice isoforms in the developing and adult brain. PLoS One. 2010;5(9):e12924.

27. Chung DW, Wills ZP, Fish KN, Lewis DA. Developmental pruning of excitatory synaptic inputs to parvalbumin interneurons in monkey prefrontal cortex. Proc Natl Acad Sci U S A. 2017;114(4):E629-E37.

28. Murakami M, Ohba T, Xu F, Satoh E, Miyoshi I, Suzuki T, et al. Modified sympathetic nerve system activity with overexpression of the voltage-dependent calcium channel beta3 subunit. J Biol Chem. 2008;283(36):24554-60.

29. Takahashi K, Tanaka A, Hara M, Nakanishi S. The primary structure and gene organization of human substance P and neuromedin K receptors. Eur J Biochem. 1992;204(3):1025-33.

30. Steinhoff MS, von Mentzer B, Geppetti P, Pothoulakis C, Bunnett NW. Tachykinins and their receptors: contributions to physiological control and the mechanisms of disease. Physiol Rev. 2014;94(1):265-301.

31. Watson LM, Bamber E, Schnekenberg RP, Williams J, Bettencourt C, Lickiss J, et al. Dominant Mutations in GRM1 Cause Spinocerebellar Ataxia Type 44. Am J Hum Genet. 2017;101(5):866.

32. Scott GD, Fryer AD. Role of parasympathetic nerves and muscarinic receptors in allergy and asthma. Chem Immunol Allergy. 2012;98:48-69.

33. Arikawa K, Takuwa N, Yamaguchi H, Sugimoto N, Kitayama J, Nagawa H, et al. Ligand-dependent inhibition of B16 melanoma cell migration and invasion via endogenous S1P2 G protein-coupled receptor. Requirement of inhibition of cellular RAC activity. J Biol Chem. 2003;278(35):32841-51.

34. Lukomska A, Dobrzanski G, Liguz-Lecznar M, Kossut M. Somatostatin receptors (SSTR1-5) on inhibitory interneurons in the barrel cortex. Brain Struct Funct. 2020;225(1):387-401.

35. Santiago C, Labrador JP, Bashaw GJ. The homeodomain transcription factor Hb9 controls axon guidance in Drosophila through the regulation of Robo receptors. Cell Rep. 2014;7(1):153-65.

36. Moore AR, Filipovic R, Mo Z, Rasband MN, Zecevic N, Antic SD. Electrical excitability of early neurons in the human cerebral cortex during the second trimester of gestation. Cereb Cortex. 2009;19(8):1795-805.

37. Moore AR, Zhou WL, Jakovcevski I, Zecevic N, Antic SD. Spontaneous electrical activity in the human fetal cortex in vitro. J Neurosci. 2011;31(7):2391-8.

38. Birnbaumer L, Zhu X, Jiang M, Boulay G, Peyton M, Vannier B, et al. On the molecular basis and regulation of cellular capacitative calcium entry: Roles for Trp proteins. Proceedings of the National Academy of Sciences. 1996;93(26):15195-202.

39. Belkacemi A, Hui X, Wardas B, Laschke MW, Wissenbach U, Menger MD, et al. IP3 Receptor-Dependent Cytoplasmic Ca(2+) Signals Are Tightly Controlled by Cavbeta3. Cell Rep. 2018;22(5):1339-49.

40. Decaillot FM, Kazmi MA, Lin Y, Ray-Saha S, Sakmar TP, Sachdev P. CXCR7/CXCR4 heterodimer constitutively recruits beta-arrestin to enhance cell migration. J Biol Chem. 2011;286(37):32188-97.

41. Chapman NA, Dupre DJ, Rainey JK. The apelin receptor: physiology, pathology, cell signalling, and ligand modulation of a peptide-activated class A GPCR. Biochem Cell Biol. 2014;92(6):431-40.

42. Brighton PJ, Szekeres PG, Willars GB. Neuromedin U and its receptors: structure, function, and physiological roles. Pharmacol Rev. 2004;56(2):231-48.

43. Lepski G, Jannes C, Nikkhah G, Bischofberger J. cAMP promotes the differentiation of neural progenitor cells in vitro via modulation of voltage-gated calcium channels. Frontiers in Cellular Neuroscience. 2013;7(155).

44. Bando Y, Irie K, Shimomura T, Umeshima H, Kushida Y, Kengaku M, et al. Control of Spontaneous Ca2+ Transients Is Critical for Neuronal Maturation in the Developing Neocortex. Cerebral Cortex. 2016;26(1):106-17.

45. Dessaud E, McMahon AP, Briscoe J. Pattern formation in the vertebrate neural tube: a sonic hedgehog morphogen-regulated transcriptional network. Development. 2008;135(15):2489-503.

46. Nam H, Jeon S, An H, Yoo J, Lee HJ, Lee SK, et al. Critical roles of ARHGAP36 as a signal transduction mediator of Shh pathway in lateral motor columnar specification. Elife. 2019;8.

47. Nakamura F, Kumeta K, Hida T, Isono T, Nakayama Y, Kuramata-Matsuoka E, et al. Amino- and carboxyl-terminal domains of Filamin-A interact with CRMP1 to mediate Sema3A signalling. Nat Commun. 2014;5:5325.

48. Dimos JTR, K.T.; Niakan, K.K.; Weisenthal, L.M.; Mitsumoto, H.; Chung, W.; Croft, G.F.; Saphier, G.; Leibel, R.; Goland, R.; Wichterle, H.; Henderson, C.E.; Eggan, K. Induced Pluripotent Stem Cells Generated from Patients with ALS Can Be Differentiated into Motor Neurons. Science. 2008;321(5893):1218-21.

751 49. McCorry LK. Physiology of the autonomic nervous system. Am J Pharm Educ.
752 2007;71(4):78.

753 50. Blankenship AG, Feller MB. Mechanisms underlying spontaneous patterned activity in
754 developing neural circuits. Nat Rev Neurosci. 2010;11(1):18-29.

755 51. McGleenon BM, Dynan KB, Passmore AP. Acetylcholinesterase inhibitors in
756 Alzheimer's disease. Br J Clin Pharmacol. 1999;48(4):471-80.

757 52. Pagano G, Rengo G, Pasqualetti G, Femminella GD, Monzani F, Ferrara N, et al.
758 Cholinesterase inhibitors for Parkinson's disease: a systematic review and meta-analysis. J
759 Neurol Neurosurg Psychiatry. 2015;86(7):767-73.

760 53. Hampel H, Mesulam MM, Cuello AC, Farlow MR, Giacobini E, Grossberg GT, et al.
761 The cholinergic system in the pathophysiology and treatment of Alzheimer's disease. Brain.
762 2018;141(7):1917-33.

763 54. Kaur S, Singh S, Chahal KS, Prakash A. Potential pharmacological strategies for the
764 improved treatment of organophosphate-induced neurotoxicity. Can J Physiol Pharmacol.
765 2014;92(11):893-911.

766 55. Colovic MB, Krstic DZ, Lazarevic-Pasti TD, Bondzic AM, Vasic VM.
767 Acetylcholinesterase inhibitors: pharmacology and toxicology. Curr Neuropharmacol.
768 2013;11(3):315-35.

769 56. Lo CC, Chain PS. Rapid evaluation and quality control of next generation sequencing
770 data with FaQCs. BMC Bioinformatics. 2014;15:366.

771 57. Shakya MC, P. PiReT Pipeline for Reference based Transcriptomics.

772 58. Love MI, Huber W, Anders S. Moderated estimation of fold change and dispersion for
773 RNA-seq data with DESeq2. Genome Biol. 2014;15(12):550.

774 59. Kanehisa M. Toward understanding the origin and evolution of cellular organisms.
775 Protein Sci. 2019;28(11):1947-51.

776 60. Kanehisa M, Goto S. KEGG: kyoto encyclopedia of genes and genomes. Nucleic Acids
777 Res. 2000;28(1):27-30.

778

779 **Figure Legends**

780 **Figure 1.** Differentiation of WTC-11 induced pluripotent stem cells (iPSC) into motor neurons
781 (MN). **(A)** Schematic diagram of the overall experimental design. Shown are the small molecule
782 stimuli for each developmental stage and the corresponding morphological changes in the course
783 of iPSC conversion into MN. The scale bar for the phase contrast images is 400

μm; **(B)** Representative immunofluorescence images of key pluripotency (Oct4) and pan-neuronal (Nestin, Pax6, and β-III tubulin) biomarkers indicated at efficient iPSC differentiation into neuronal stem cells (NSC) at day $7^{th}$ post-induction (accumulation of Nestin is shown in orange). Upregulation of Pax6 and β-III tubulin (shown in green) at day 13 of iPSC induction marked the formation of motor neuron progenitor (MNP) cells. **(C)** Immunostaining of neuronal structural proteins (beta-III-tubulin in green, MAP2 in orange), motor neuron specific markers (HB9 and ChAT in green), and synaptic vesicles protein (Synaptophysin in green) showed a pure population of mature MN at day 28 post-stimulation of iPSC. Scale bar: 100 μm.

**Figure 2.** Electrophysiological analysis of (MNs). **(A)** Time-dependent increase of spontaneous action potential (AP) spikes generated by MNs and recorded from a representative electrode (one of 144) on a multi-electrode (MEA) chip. MN were plated on the MEA chip at 18 days post-chemical induction of iPSC (D18) and electrophysiological activity was recorded at the indicated time points of MN maturation (D22-D31) for 1 min. The frequency of AP spikes **(B)** and the percentage of spikes in the burst **(C)** dramatically increased within the neuronal networks over time. Shown are the mean and standard error from 12 electrodes at each sampling day post iPSC induction.

**Figure 3.** Transcriptome analysis of cellular responses to MN maturation. **(A)** Principal component analysis of all samples, n=3; **(B)** Histogram of differentially expressed genes (DEGs) (adjusted $p < 0.0002$, fold change > 3) among D7 - D28 samples in the pairwise comparison with D0; **(C)** Histogram of DEGs in pairwise comparisons between adjacent timepoints (D0-D7, D7-D13, D13-18, D18-28).

805 **Figure 4**. Bioinformatics analysis of transcriptomic data. (A) Gene ontology (GO) analysis of
806 iPSCs and MNs as determined by the NCBI Database for Annotation, Visualization and Integrated
807 Discovery (DAVID). The top four significant GO terms of upregulated and downregulated genes
808 are listed, ranked by p-value, when comparing D0 iPSCs and D28 MNs. (B) OPaver analysis of
809 12 KEGG pathways ranked by the number of DEG during the chemical reprogramming of iPSCs
810 into MNs: Pathways in cancer; Neuroactive ligand-receptor interaction; MAPK-signaling
811 pathway; Axon guidance; Ras signaling pathway; PI3K-Akt signaling pathway; Calcium
812 signaling pathway; Rap1 signaling pathway; cAMP signaling pathway; Transcriptional mis-
813 regulation in cancer; Singling pathways regulating pluripotency of stem cells; and Cholinergic
814 synapse.

815 **Figure 5.** Differential gene expression in key signaling pathways shaping MN differentiation.
816 Gene transcript levels were determined by global RNA-seq analysis of **(A)** TGFβ, **(B)** Notch, and
817 **(C)** Sonic Hedgehog (Shh) pathways. Fold change was calculated relative to RNA reads in iPSC
818 (D0). The statistics (average value and standard error) were derived from three independent
819 biological replicas with $p<0.001$ determined by R-statistical analysis package.

820 **Figure 6.** Comparative analysis of differential gene expression of key tissue development markers
821 by RT-qPCR (gray) and RNA-seq (black). Pluripotency and NSC markers validated include **(A)**
822 Oct4, transcription factor that maintains self-renewal and pluripotency; **(B)** Nestin, a filament
823 protein marker of neural stem cells; **(C)** Pax6, a transcription factor that drives neurogenesis; and
824 **(D)** NgN2, a neuronal-specific transcription factor. Motor neuron specification markers validated
825 include **(E)** Isl1, a transcription factor required for motor neuron generation; **(F)** Map2, a neuron-
826 specific cytoskeletal protein; **(G)** HB9, an early marker of cholinergic neurons; and **(H)** ChAT, an
827 enzyme required for acetylcholine synthesis. Shown are the averages and standard error from three

828 independent biological replicas from the iPSC to MN differentiation trajectory. The RNA-Seq
829 transcripts were normalized to the total read per analyzed sample (in FPKM: fragments per
830 kilobase per million mapped fragments) and the transcript levels determined by RT-qPCR were
831 normalized to GAPDH as the endogenous sample control. Fold change was calculated for each
832 developmental stage relative to transcript levels in iPSC (D0). Statistical significance ($p < 1.5e-6$)
833 was determined with Student t-test.

834

835 **Tables**

836 **Table 1: DEGs identified in KEGG pathway: MAPK-signaling.** Differential expression
837 indicates the average $log_2$-fold change in RNA-Seq transcript levels from three independent
838 experiments at each sampling period: D7 vs D0, D13 vs D7, D18 v D13, and D28 v D18. The p-
839 values were $\leq 0.001$. Negative $log_2$-fold change corresponds to gene downregulation and the
840 positive values indicate gene activation.

| **MAPK-signaling pathway** | | | |
|---|---|---|---|
| **Gene ID** | **Description** | **Differential expression** | **Time** |
| CACNA1B | voltage-dependent calcium channel N type alpha-1B | -1.834598101 | D0-D7 |
| CACNA2D1 | voltage-dependent calcium channel alpha-2/delta-1 | -5.013073193 | D0-D7 |
| CACNB3 | voltage-dependent calcium channel beta-3 | 1.96153735 | D0-D7 |
| CACNG5 | voltage-dependent calcium channel gamma-5 | -3.611690367 | D0-D7 |
| CACNG7 | voltage-dependent calcium channel gamma-7 | -2.217348209 | D0-D7 |
| CACNG8 | voltage-dependent calcium channel gamma-8 | -3.68477059 | D0-D7 |
| FGF2 | fibroblast growth factor 2 | -1.519463128 | D0-D7 |

| | | | |
|---|---|---|---|
| KITLG | KIT ligand | 2.167299479 | D0-D7 |
| NTRK2 | neurotrophic tyrosine kinase receptor type 2 | 8.559108654 | D0-D7 |
| KIT | proto-oncogene tyrosine-protein kinase Kit | 2.471526791 | D0-D7 |
| FLT1 | MS-like tyrosine kinase 1 | -6.287270931 | D0-D7 |
| KDR | kinase insert domain protein receptor | -5.882467261 | D0-D7 |
| TGFB2 | transforming growth factor beta-2 | 2.871123317 | D0-D7 |
| RASGRP2 | RAS guanyl-releasing protein 2 | -3.455335916 | D0-D7 |
| GNG12 | guanine nucleotide-binding protein G(I)/G(S)/G(O) subunit gamma-12 | -2.188972021 | D0-D7 |
| MYC | Myc proto-oncogene protein | -2.952930394 | D0-D7 |
| MECOM | ecotropic virus integration site 1 protein | 3.315425714 | D0-D7 |
| PPM1B | protein phosphatase 1B | -1.591315588 | D0-D7 |
| ERBB4 | receptor tyrosine-protein kinase erbB-4 | 4.531919812 | D7-D13 |
| CACNA1B | voltage-dependent calcium channel N type alpha-1B | 1.88048051 | D7-D13 |
| CACNA2D3 | voltage-dependent calcium channel alpha-2/delta-3 | 3.068907158 | D7-D13 |
| NTRK1 | neurotrophic tyrosine kinase receptor type 1 | 4.469959879 | D7-D13 |
| TGFB2 | transforming growth factor beta-2 | 2.803343326 | D7-D13 |
| KIT | proto-oncogene tyrosine-protein kinase Kit | -2.467841933 | D13-D18 |
| CACNG5 | voltage-dependent calcium channel gamma-5 | 4.656489914 | D13-D18 |
| FGFR4 | fibroblast growth factor receptor 4 | -3.26316459 | D13-D18 |
| CACNA1E | voltage-dependent calcium channel R type alpha-1E | 3.425325465 | D18-D28 |
| CACNG2 | voltage-dependent calcium channel gamma-2 | 3.474133324 | D18-D28 |
| CACNG8 | voltage-dependent calcium channel gamma-8 | 3.189789 | D18-D28 |
| KITLG | KIT ligand | 2.028343818 | D18-D28 |
| EGFR | epidermal growth factor receptor | -2.084730311 | D18-D28 |
| FGFR1 | fibroblast growth factor receptor 1 | -2.081183963 | D18-D28 |
| FGFR2 | fibroblast growth factor receptor 2 | -3.256153332 | D18-D28 |

| | | | |
|---|---|---|---|
| FGFR3 | fibroblast growth factor receptor 3 | -5.009604609 | D18-D28 |
| KDR | kinase insert domain protein receptor | 3.118215378 | D18-D28 |
| IL1RAP | interleukin 1 receptor accessory protein | 3.502622162 | D18-D28 |
| PRKCB | classical protein kinase C beta type | 1.642454101 | D18-D28 |
| PTPRR | receptor-type tyrosine-protein phosphatase R | 2.837257876 | D18-D28 |
| PTPN5 | tyrosine-protein phosphatase non-receptor type 5 | 2.472116702 | D18-D28 |
| MAPKAPK2 | mitogen-activated protein kinase-activated protein kinase 2 | -1.628879059 | D18-D28 |
| CDC25B | M-phase inducer phosphatase 2 | -3.052843516 | D18-D28 |
| MAP3K5 | mitogen-activated protein kinase kinase kinase 5 | 1.972512785 | D18-D28 |

**Table 2: DEGs identified in KEGG pathway: Calcium signaling.** Differential expression indicates the average $\log_2$-fold change in RNA-Seq transcript levels from three independent experiments at each sampling period: D7 vs D0, D13 vs D7, D18 v D13, and D28 v D18. The p-values were $\leq 0.001$. Negative $\log_2$-fold change corresponds to gene downregulation and the positive values indicate gene activation.

| **Calcium signaling pathway** | | | |
|---|---|---|---|
| **Gene ID** | **Description** | **Differential expression** | **Time** |
| HTR7 | 5-hydroxytryptamine receptor 7 | -5.492892685 | D0-D7 |
| CACNA1B | voltage-dependent calcium channel N type alpha-1B | -1.834598101 | D0-D7 |
| CXCR4 | C-X-C chemokine receptor type 4 | 4.604478969 | D0-D7 |
| ADCY2 | adenylate cyclase 2 | -3.460253861 | D0-D7 |
| STIM1 | stromal interaction molecule 1 | 1.834422349 | D0-D7 |
| VDAC1 | voltage-dependent anion channel protein 1 | -1.32731076 | D0-D7 |
| GNA14 | guanine nucleotide-binding protein subunit alpha-14 | -5.014275635 | D0-D7 |

| | | | |
|---|---|---|---|
| TRDN | triadin | -4.320486512 | D0-D7 |
| RYR2 | ryanodine receptor 2 | -4.07053211 | D0-D7 |
| RYR3 | ryanodine receptor 3 | 1.71133494 | D0-D7 |
| ITPR2 | inositol 1,4,5-triphosphate receptor type 2 | -3.699823272 | D0-D7 |
| ITPR3 | inositol 1,4,5-triphosphate receptor type 3 | -2.406497059 | D0-D7 |
| ERBB4 | receptor tyrosine-protein kinase erbB-4 | 4.531919812 | D7-D13 |
| CACNA1B | voltage-dependent calcium channel N type alpha-1B | 1.88048051 | D13-D18 |
| CACNA1E | voltage-dependent calcium channel R type alpha-1E | 3.425325465 | D13-D18 |
| GRIN2A | glutamate receptor ionotropic, NMDA 2A | 2.854753149 | D13-D18 |
| P2RX3 | P2X purinoceptor 3 | 2.552456853 | D13-D18 |
| CAMK4 | calcium/calmodulin-dependent protein kinase IV | 1.41910402 | D13-D18 |
| CHRM3 | muscarinic acetylcholine receptor M3 | 3.978819163 | D18-D28 |
| HTR7 | 5-hydroxytryptamine receptor 7 | 3.808433488 | D18-D28 |
| GRIN1 | glutamate receptor ionotropic, NMDA 1 | 3.726336735 | D18-D28 |
| GRIN2D | glutamate receptor ionotropic, NMDA 2D | 2.087932817 | D18-D28 |
| CHRM2 | muscarinic acetylcholine receptor M2 | 3.383752478 | D18-D28 |
| ADRA1A | adrenergic receptor alpha-1A | 4.207285974 | D18-D28 |
| TACR3 | tachykinin receptor 3 | 2.111829478 | D18-D28 |
| GRM1 | metabotropic glutamate receptor 1 | 3.134222868 | D18-D28 |
| EGFR | epidermal growth factor receptor | -2.084730311 | D18-D28 |
| GNAL | guanine nucleotide-binding protein G(olf) subunit alpha | 1.685044809 | D18-D28 |
| ADCY2 | adenylate cyclase 2 | 3.240853085 | D18-D28 |
| STIM2 | stromal interaction molecule 2 | 1.158068159 | D18-D28 |
| RYR2 | ryanodine receptor 2 | 4.896050853 | D18-D28 |
| PRKCB | classical protein kinase C beta type | 1.642454101 | D18-D28 |

847

**Table 3: DEGs identified in KEGG pathway: Neuroactive ligand-receptor interaction.** Differential expression indicates the average $log_2$-fold change in RNA-Seq transcript levels from three independent experiments at each sampling period: D7 vs D0, D13 vs D7, D18 v D13, and D28 v D18. The p-values were ≤ 0.001. Negative $log_2$-fold change corresponds to gene downregulation and the positive values indicate gene activation.

| **Neuroactive ligand-receptor interaction** | | | |
|---|---|---|---|
| **Gene ID** | **Description** | **Differential expression** | **Time** |
| APLNR | apelin receptor | 4.656030708 | D0-D7 |
| NMUR2 | neuromedin U receptor 2 | 8.490690944 | D0-D7 |
| F2 | coagulation factor II (thrombin) | 2.589060962 | D0-D7 |
| CNR1 | cannabinoid receptor 1 | 2.81817017 | D0-D7 |
| S1PR1 | sphingosine 1-phosphate receptor 1 | 5.38497247 | D0-D7 |
| GRM4 | metabotropic glutamate receptor 4 | -3.861684955 | D0-D7 |
| GRIN2B | glutamate receptor ionotropic, NMDA 2B | -2.895136106 | D0-D7 |
| CHRNA3 | nicotinic acetylcholine receptor alpha-3 | 2.7938378 | D0-D7 |
| HTR7 | 5-hydroxytryptamine receptor 7 | -5.492892685 | D0-D7 |
| CHRNB4 | nicotinic acetylcholine receptor beta-4 | 4.925250798 | D0-D7 |
| GRIA1 | glutamate receptor 1 | 3.01762919 | D0-D7 |
| GRIA4 | glutamate receptor 4 | -2.647220311 | D0-D7 |
| GRIK1 | glutamate receptor, ionotropic 41ainite 1 | 2.276415318 | D0-D7 |
| GRIK4 | glutamate receptor, ionotropic 41ainite 4 | -3.020412525 | D0-D7 |
| GRID2 | glutamate receptor delta-2 subunit | -5.40793957 | D0-D7 |
| GLRA2 | glycine receptor alpha-2 | 1.792820308 | D0-D7 |
| GLRB | glycine receptor beta | 3.452103236 | D0-D7 |
| NR3C1 | glucocorticoid receptor | -2.452514385 | D0-D7 |

| | | | |
|---|---|---|---|
| GHR | growth hormone receptor | 2.976564346 | D0-D7 |
| CNR1 | cannabinoid receptor 1 | 2.626395057 | D7-D13 |
| NR3C1 | glucocorticoid receptor | 3.341402421 | D7-D13 |
| GRIN2A | glutamate receptor ionotropic, NMDA 2A | 2.854753149 | D13-D18 |
| CHRNA4 | nicotinic acetylcholine receptor alpha-4 | 2.830329136 | D13-D18 |
| P2RX3 | P2X purinoceptor 3 | 2.552456853 | D13-D18 |
| GRIA2 | glutamate receptor 2 | 3.273675604 | D13-D18 |
| GRIA4 | glutamate receptor 4 | 2.416455621 | D13-D18 |
| ADCYAP1R1 | pituitary adenylate cyclase-activating polypeptide type I receptor | 2.615605165 | D13-D18 |
| CHRM2 | muscarinic acetylcholine receptor M2 | 3.383752478 | D18-D28 |
| CHRM3 | muscarinic acetylcholine receptor M3 | 3.978819163 | D18-D28 |
| ADRA1A | adrenergic receptor alpha-1A | 4.207285974 | D18-D28 |
| DRD2 | dopamine receptor D2 | -2.728065758 | D18-D28 |
| HTR7 | 5-hydroxytryptamine receptor 7 | 3.808433488 | D18-D28 |
| NMU | neuromedin U | -2.62455439 | D18-D28 |
| NPY5R | neuropeptide Y receptor type 5 | 3.804748523 | D18-D28 |
| HCRTR2 | hypocretin (orexin) receptor 2 | 3.98239527 | D18-D28 |
| SSTR1 | somatostatin receptor 1 | 6.807432954 | D18-D28 |
| TAC1 | tachykinin 1 | 3.869735499 | D18-D28 |
| TACR3 | tachykinin receptor 3 | 2.111829478 | D18-D28 |
| PTGER4 | prostaglandin E receptor 4 | 2.824782168 | D18-D28 |
| GPR50 | G protein-coupled receptor 50 | 4.747091061 | D18-D28 |
| LPAR1 | lysophosphatidic acid receptor 1 | 1.500777066 | D18-D28 |
| S1PR1 | sphingosine 1-phosphate receptor 1 | 2.506524278 | D18-D28 |
| ADCYAP1R1 | pituitary adenylate cyclase-activating polypeptide type I receptor | -2.231972171 | D18-D28 |

| | | | |
|---|---|---|---|
| GRM1 | metabotropic glutamate receptor 1 | 3.134222868 | D18-D28 |
| GRIN1 | glutamate receptor ionotropic, NMDA 1 | 3.726336735 | D18-D28 |
| GRIN2D | glutamate receptor ionotropic, NMDA 2D | 2.087932817 | D18-D28 |
| GRIN3A | glutamate receptor ionotropic, NMDA 3A | 2.914543821 | D18-D28 |
| CHRNA3 | nicotinic acetylcholine receptor alpha-3 | -2.670435709 | D18-D28 |
| GRIA2 | glutamate receptor 2 | 2.698334339 | D18-D28 |
| GRIA4 | glutamate receptor 4 | 1.923861676 | D18-D28 |
| GRID2 | glutamate receptor delta-2 subunit | 4.217720694 | D18-D28 |
| GRIN2B | glutamate receptor ionotropic, NMDA 2B | 4.109294839 | D18-D28 |
| GLRA3 | glycine receptor alpha-3 | 5.577349539 | D18-D28 |
| GLRB | glycine receptor beta | 1.392250382 | D18-D28 |

**Table 4: DEGs identified in KEGG pathway: Axon guidance.** Differential expression indicates the average $log_2$-fold change in RNA-Seq transcript levels from three independent experiments at each sampling period: D7 vs D0, D13 vs D7, D18 v D13, and D28 v D18. The p-values were ≤ 0.001. Negative $log_2$-fold change corresponds to gene downregulation and the positive values indicate gene activation.

| **Axon guidance** | | | |
|---|---|---|---|
| **Gene ID** | **Description** | **Differential expression** | **Time** |
| NTNG1 | netrin-G1 | -2.536297436 | D0-D7 |
| DCC | deleted in colorectal carcinoma | 2.502983549 | D0-D7 |
| NTN1 | netrin 1 | 3.198672486 | D0-D7 |
| FYN | tyrosine-protein kinase Fyn | 1.772436052 | D0-D7 |
| RGMA | repulsive guidance molecule A | 3.097407276 | D0-D7 |

| | | | |
|---|---|---|---|
| CXCR4 | C-X-C chemokine receptor type 4 | 4.604478969 | D0-D7 |
| CXCL12 | C-X-C motif chemokine 12 | -4.220104913 | D0-D7 |
| EPHA3 | Eph receptor A3 | 3.43500774 | D0-D7 |
| EPHA4 | Eph receptor A4 | 1.860959561 | D0-D7 |
| EPHA7 | EphA7 | 2.088277014 | D0-D7 |
| EPHB2 | Eph receptor B2 | 1.873701283 | D0-D7 |
| EPHB3 | Eph receptor B3 | 5.416063376 | D0-D7 |
| ENAH | enabled | -0.89497636 | D0-D7 |
| SLIT1 | slit 1 | 5.447826267 | D0-D7 |
| ROBO2 | roundabout, axon guidance receptor 2 | -2.472827128 | D0-D7 |
| NRP1 | neuropilin 1 | 4.117109594 | D0-D7 |
| DPYSL5 | dihydropyrimidinase-like 5 | 4.921620042 | D0-D7 |
| PTCH1 | patched 1 | 3.517640353 | D0-D7 |
| BOC | brother of CDO | 4.811514207 | D0-D7 |
| BMP7 | bone morphogenetic protein 7 | 3.232399315 | D0-D7 |
| BMPR1B | bone morphogenetic protein receptor type-1B | 1.78373296 | D0-D7 |
| DCC | deleted in colorectal carcinoma | 2.626762708 | D7-D13 |
| EPHA3 | Eph receptor A3 | 2.836614823 | D7-D13 |
| PAK3 | p21-activated kinase 3 | 1.64575883 | D13-D18 |
| NTNG1 | netrin-G1 | 2.991377261 | D13-D18 |
| EPHA5 | Eph receptor A5 | 3.15278798 | D13-D18 |
| SLIT1 | slit 1 | 2.183813571 | D13-D18 |
| SLIT2 | slit 2 | 2.342825102 | D13-D18 |
| NTNG1 | netrin-G1 | 2.430765649 | D18-D28 |
| TRPC5 | transient receptor potential cation channel subfamily C member 5 | 2.464006156 | D18-D28 |
| RGS3 | regulator of G-protein signaling 3 | -1.814236062 | D18-D28 |

| | | | |
|---|---|---|---|
| CXCL12 | C-X-C motif chemokine 12 | 3.751564688 | D18-D28 |
| EPHA5 | Eph receptor A5 | 3.524159164 | D18-D28 |
| EPHA6 | Eph receptor A6 | 2.585950072 | D18-D28 |
| BOC | brother of CDO | -1.858286661 | D18-D28 |
| WNT4 | wingless-type MMTV integration site family, member 4 | 2.873234122 | D18-D28 |

859

860 **Table 5: DEGs identified in KEGG pathway: Cholinergic synapse.** Differential expression
861 indicates the average $log_2$-fold change in RNA-Seq transcript levels from three independent
862 experiments at each sampling period: D7 vs D0, D13 vs D7, D18 v D13, and D28 v D18. The p-
863 values were $\leq 0.001$. Negative $log_2$-fold change corresponds to gene downregulation and the
864 positive values indicate gene activation.

| **Cholinergic synapse** | | | |
|---|---|---|---|
| **Gene ID** | **Description** | **Differential expression** | **Time** |
| GNG12 | guanine nucleotide-binding protein G(I)/G(S)/G(O) subunit gamma-12 | -2.18897 | D0-D7 |
| CACNA1B | voltage-dependent calcium channel N type alpha-1B | -1.8346 | D0-D7 |
| KCNQ3 | potassium voltage-gated channel KQT-like subfamily member 3 | -2.96129 | D0-D7 |
| KCNJ12 | potassium inwardly-rectifying channel subfamily J member 12 | 3.350697 | D0-D7 |
| CHRNA3 | nicotinic acetylcholine receptor alpha-3 | 2.793838 | D0-D7 |
| CHRNB4 | nicotinic acetylcholine receptor beta-4 | 4.925251 | D0-D7 |
| ITPR2 | inositol 1,4,5-triphosphate receptor type 2 | -3.69982 | D0-D7 |
| ITPR3 | inositol 1,4,5-triphosphate receptor type 3 | -2.4065 | D0-D7 |

| | | | |
|---|---|---|---|
| ADCY2 | adenylate cyclase 2 | -3.4602539 | D0-D7 |
| ADCY6 | adenylate cyclase 6 | 1.892735 | D0-D7 |
| CREB5 | cyclic AMP-responsive element-binding protein 5 | 2.033579 | D0-D7 |
| FYN | tyrosine-protein kinase Fyn | 1.772436 | D0-D7 |
| CAMK4 | calcium/calmodulin-dependent protein kinase IV | 1.419104 | D7-D13 |
| ChAT | choline O-acetyltransferase | 4.392642 | D13-D18 |
| CACNA1B | voltage-dependent calcium channel N type alpha-1B | 1.880481 | D13-D18 |
| SLC5A7 | solute carrier family 5 (high affinity choline transporter), member 7 | 4.94003258 | D13-D18 |
| KCNQ2 | potassium voltage-gated channel KQT-like subfamily member 2 | 3.013059 | D13-D18 |
| CHRNA4 | nicotinic acetylcholine receptor alpha-4 | 2.830329 | D13-D18 |
| CHRM3 | muscarinic acetylcholine receptor M3 | 3.97881916 | D18-D28 |
| ChAT | choline O-acetyltransferase | 1.799457 | D18-D28 |
| ACHE | acetylcholinesterase | 2.982588 | D18-D28 |
| CHRM2 | muscarinic acetylcholine receptor M2 | 3.383752 | D18-D28 |
| SLC5A7 | solute carrier family 5 (high affinity choline transporter), member 7 | 2.363264 | D18-D28 |
| KCNQ3 | potassium voltage-gated channel KQT-like subfamily member 3 | 3.701006 | D18-D28 |
| CHRNA3 | nicotinic acetylcholine receptor alpha-3 | -2.67044 | D18-D28 |
| PRKCB | classical protein kinase C beta type | 1.642454 | D18-D28 |
| ADCY2 | adenylate cyclase 2 | 3.240853 | D18-D28 |

865

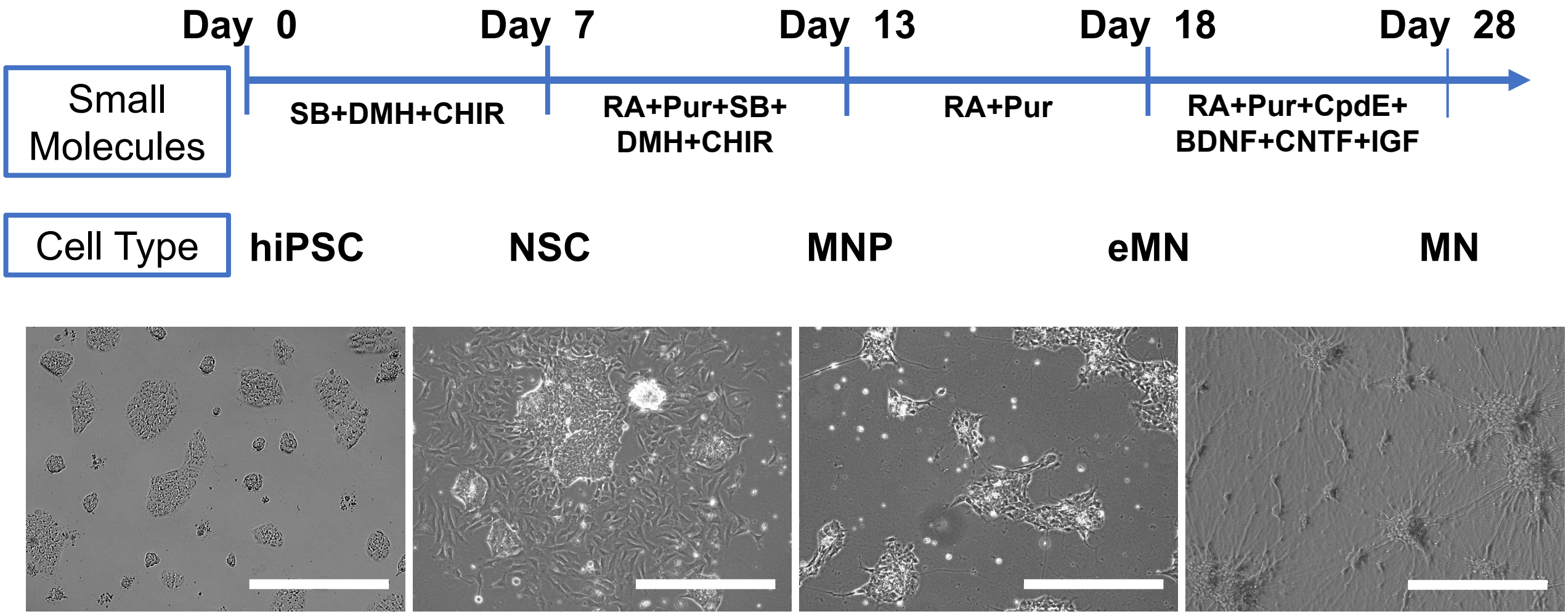
Day 0
Day 7
Day 13
Day 18
Day 28
Small Molecules
SB+DMH+CHIR
RA+Pur+SB+ DMH+CHIR
RA+Pur
RA+Pur+CpdE+ BDNF+CNTF+IGF
Cell Type
hiPSC
NSC
MNP
eMN
MN

**Figure 1 A**

# Figure 1B

D0 - iPSC

D7 - NSC

D13 - MNP

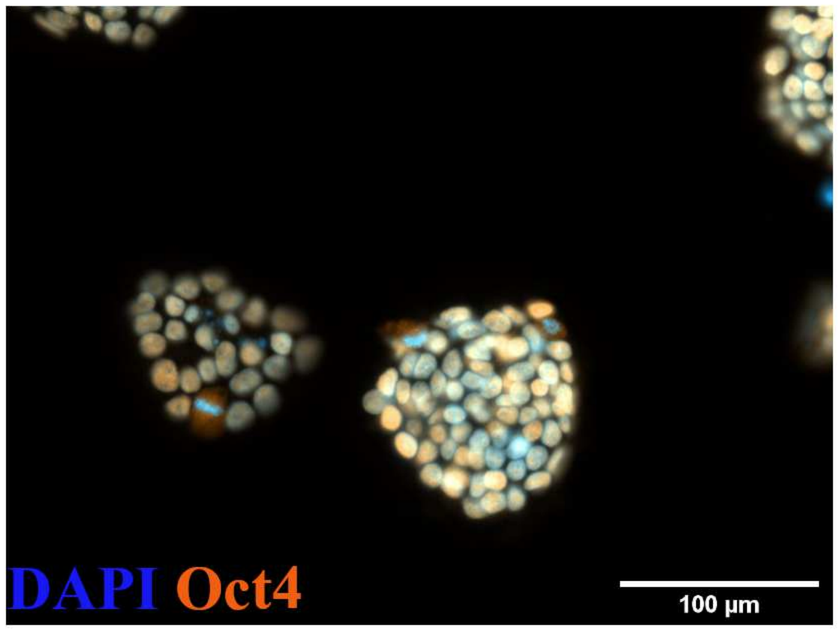


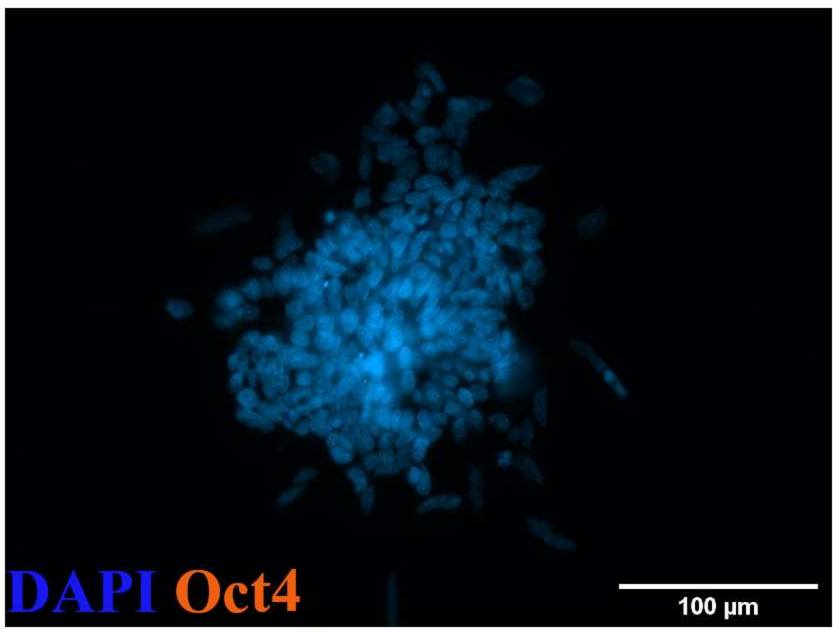


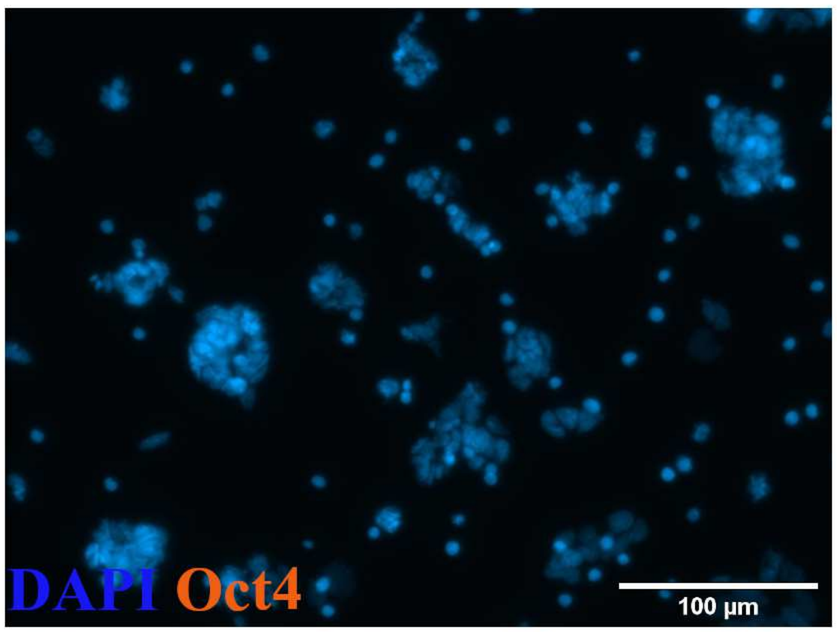


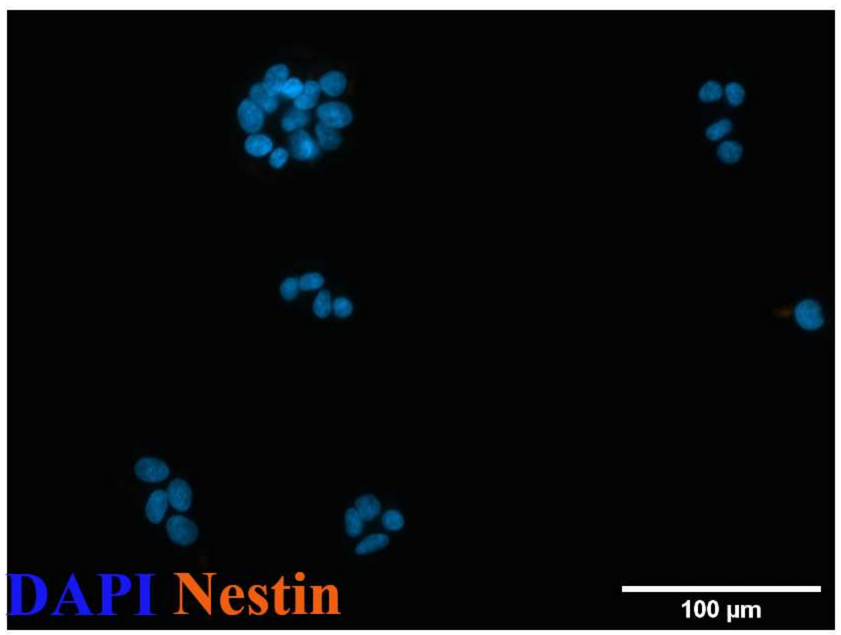


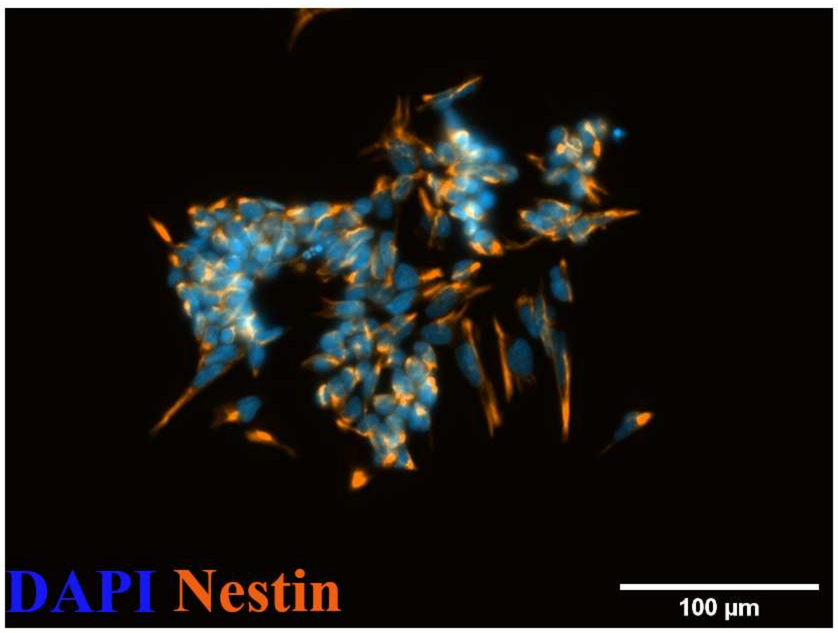


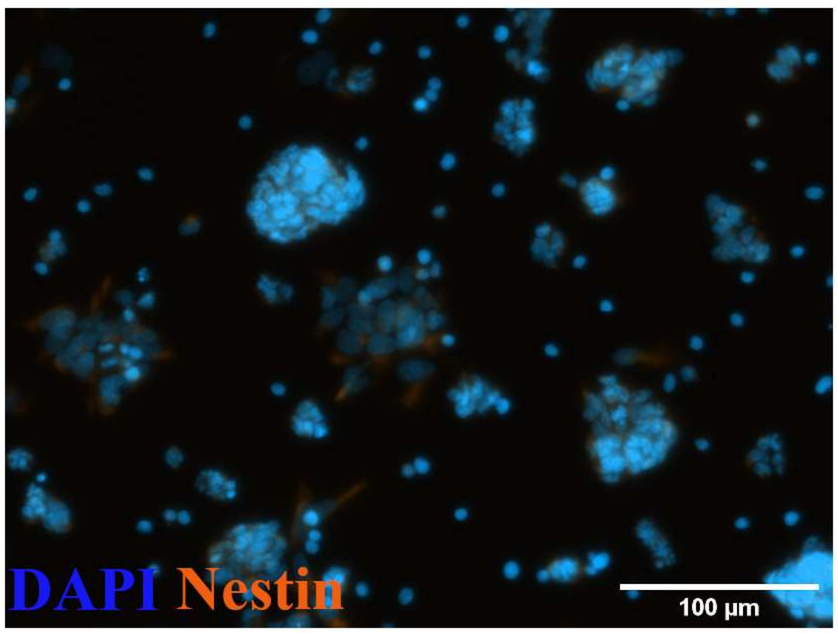


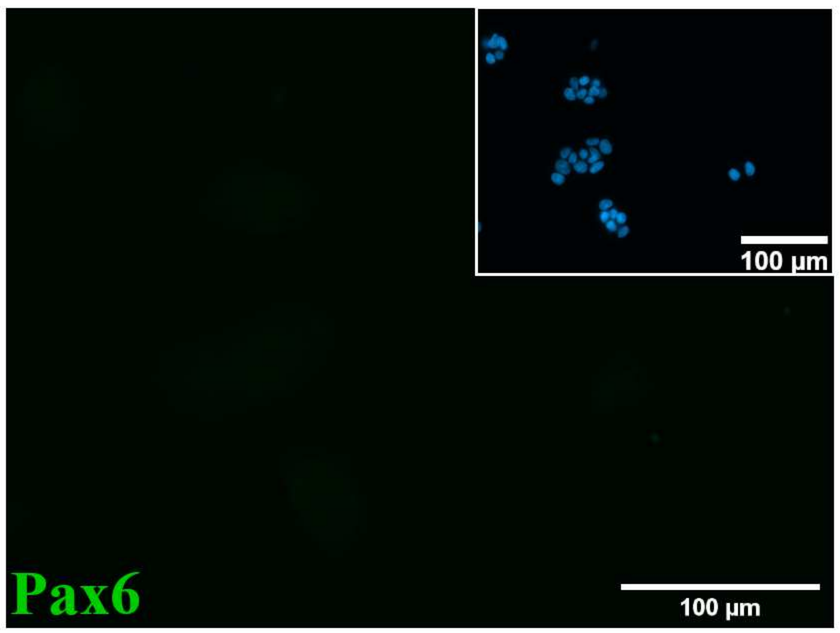


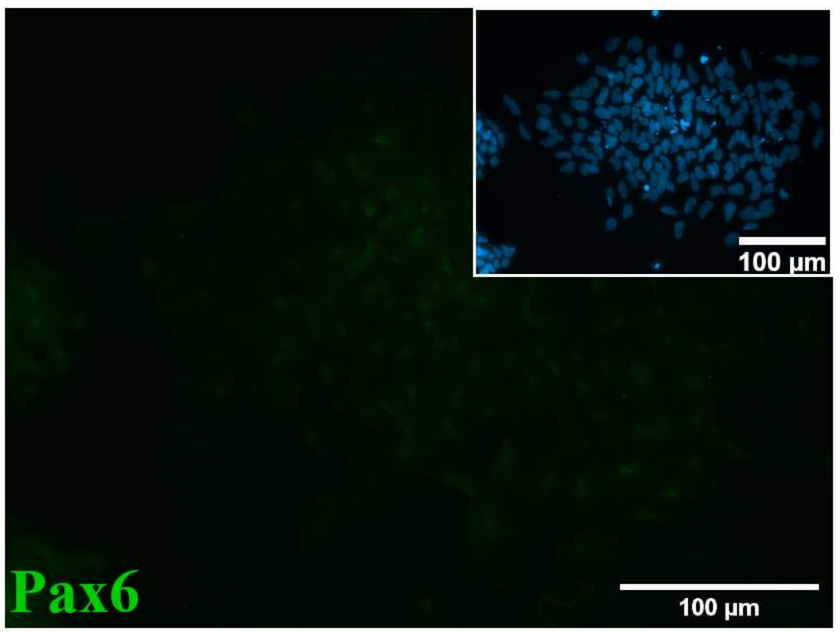


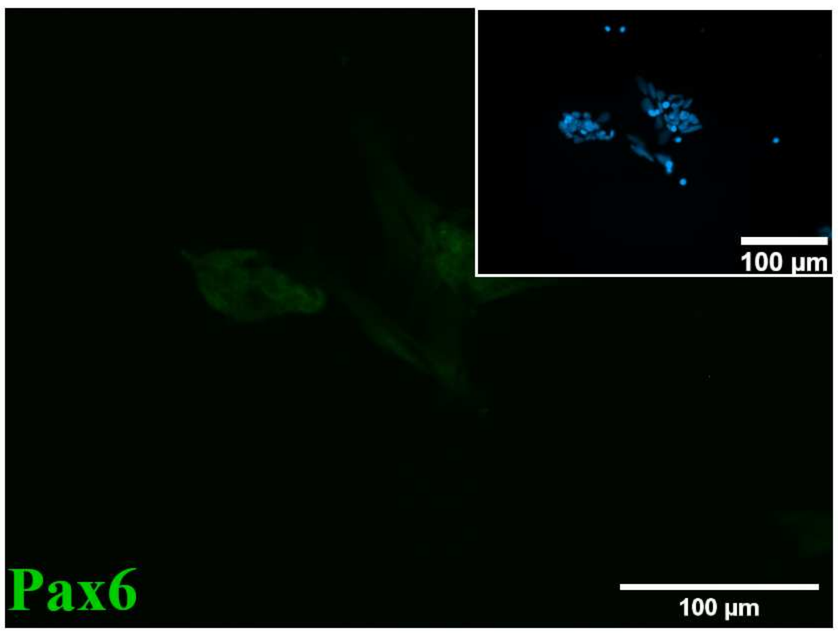


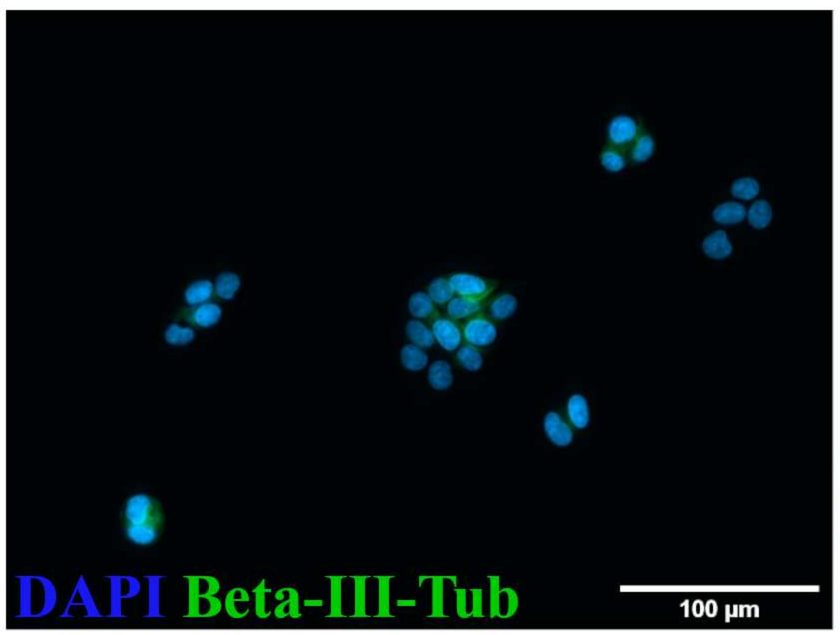


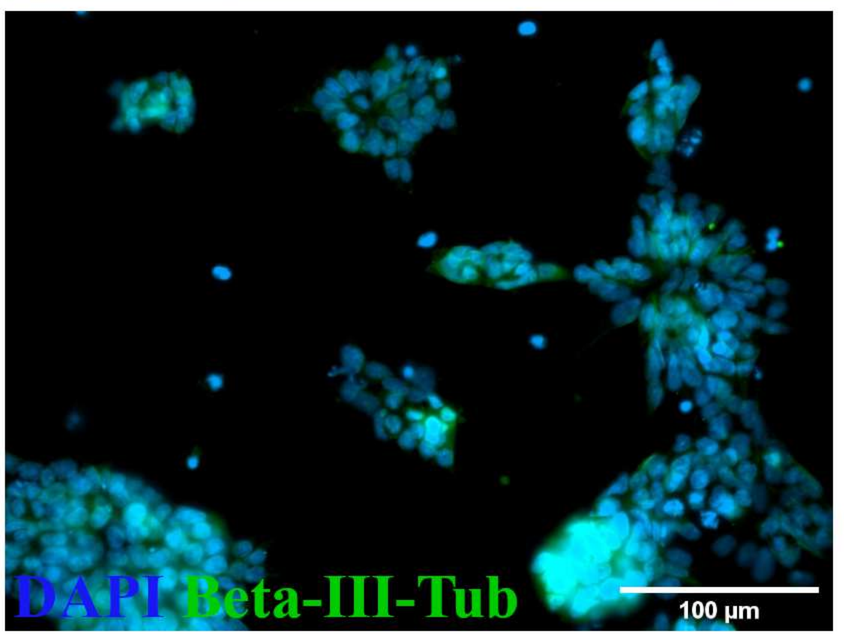


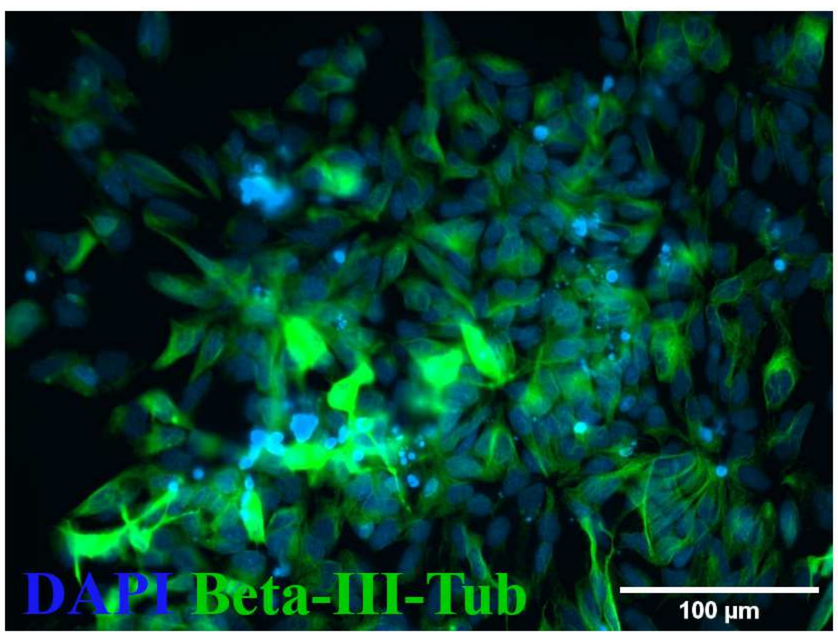

# Figure 1C

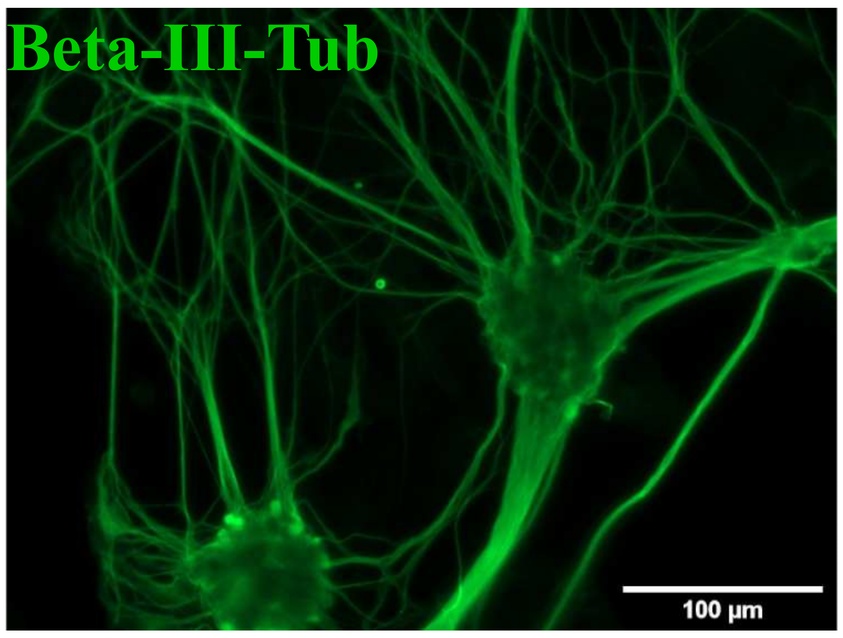
Beta-III-Tub
100 µm

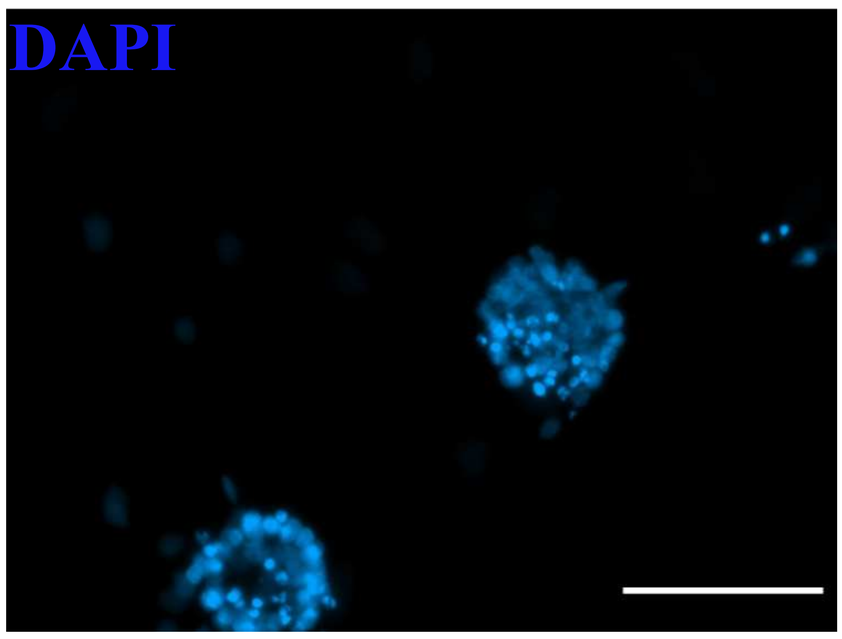
DAPI

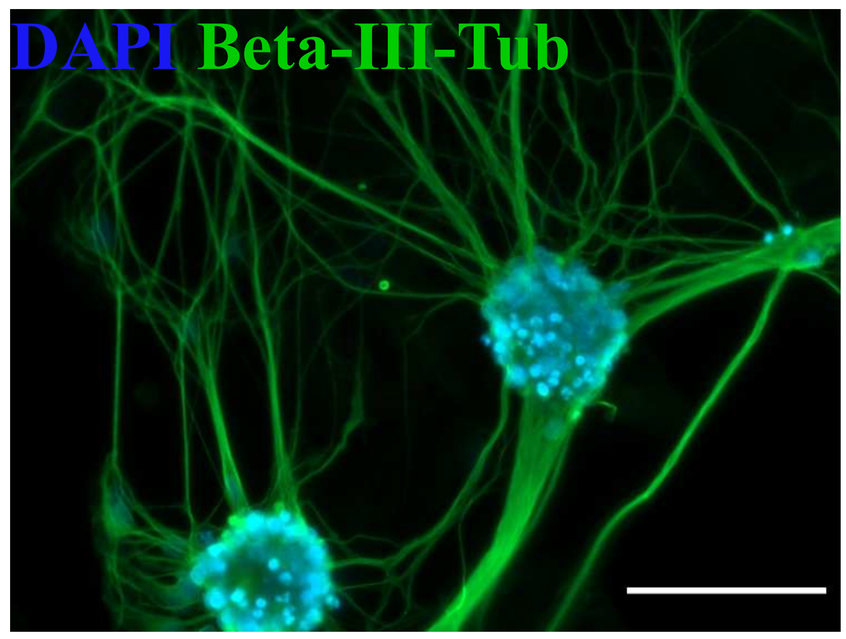
DAPI Beta-III-Tub

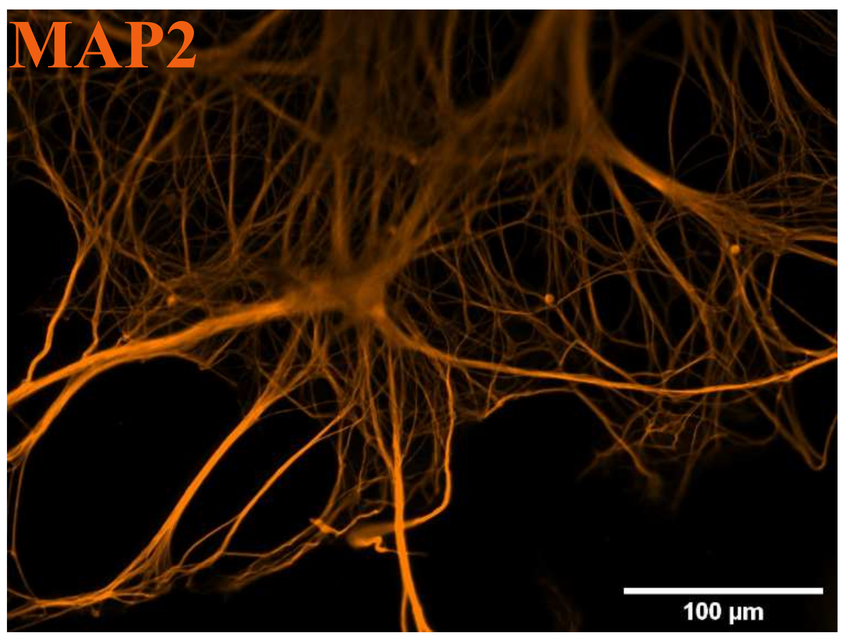
MAP2
100 µm

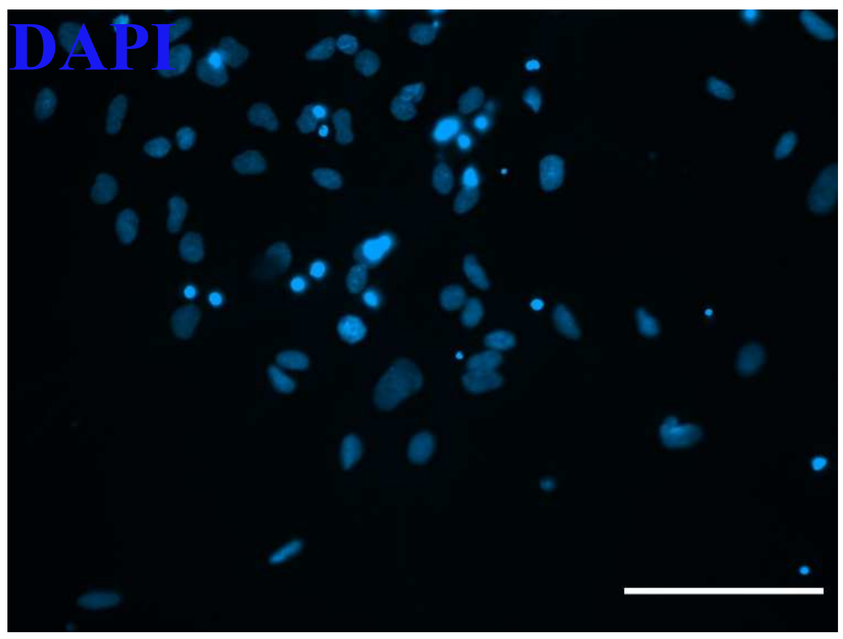
DAPI

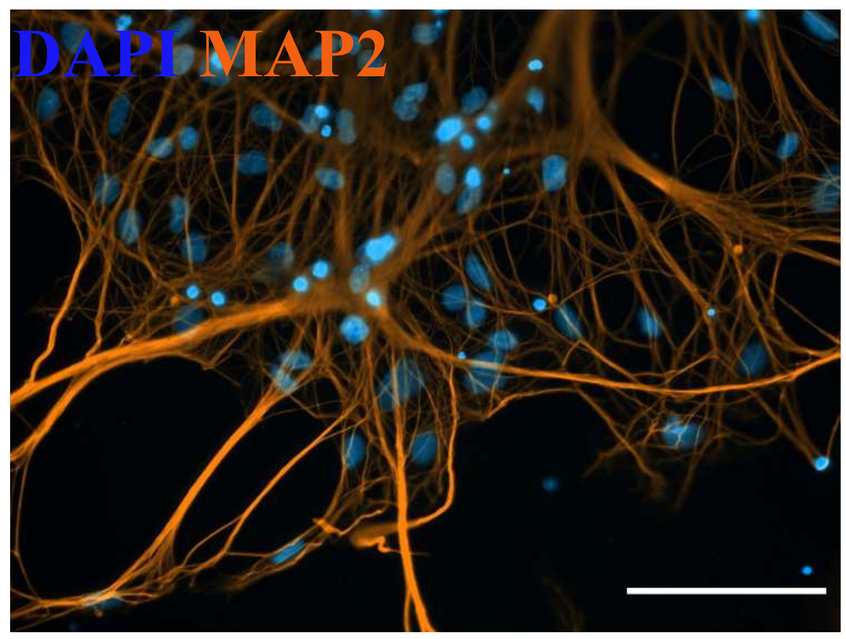
DAPI MAP2

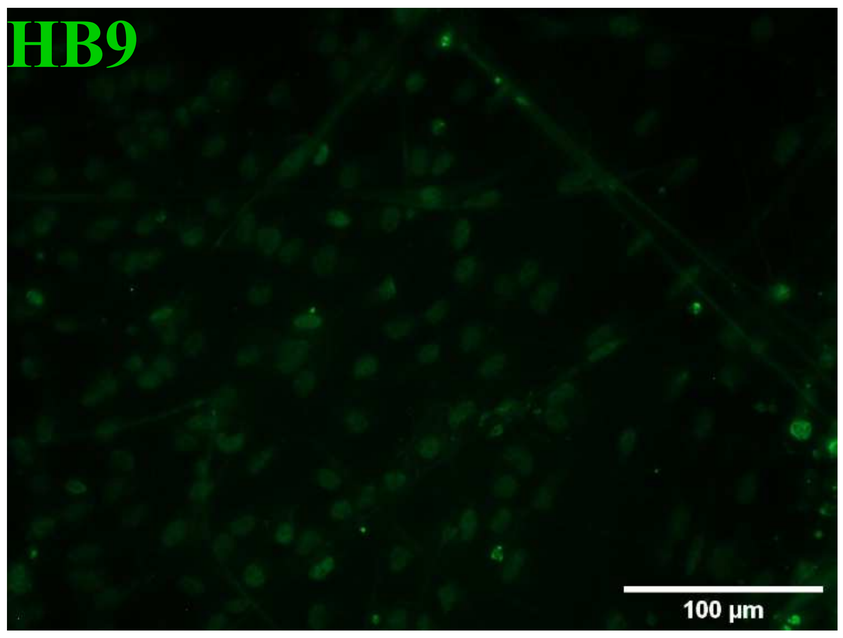
HB9
100 µm

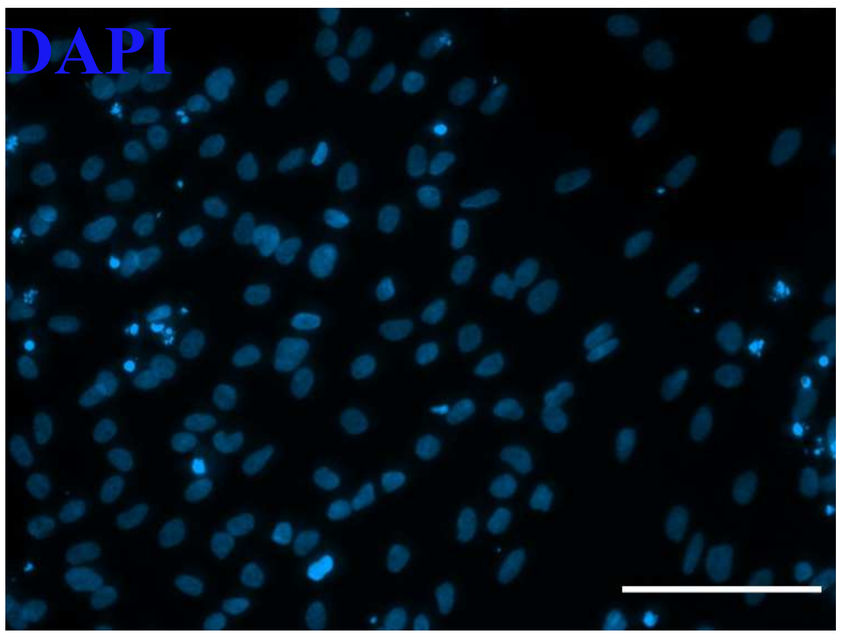
DAPI

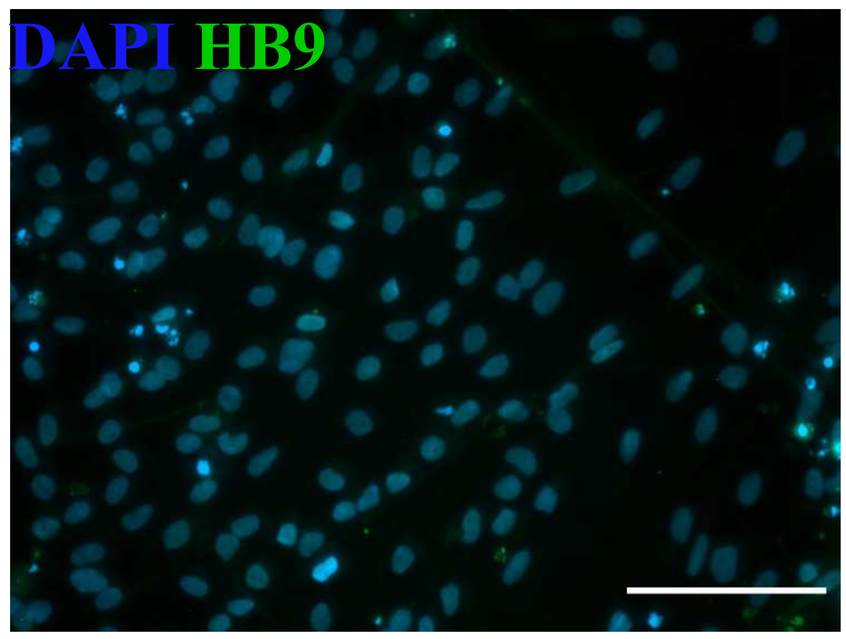
DAPI HB9

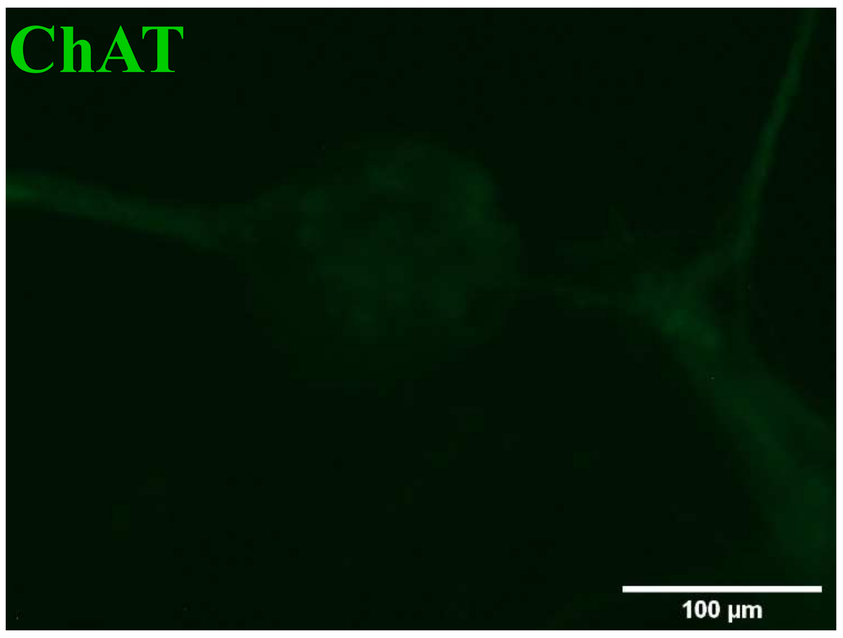
ChAT
100 µm

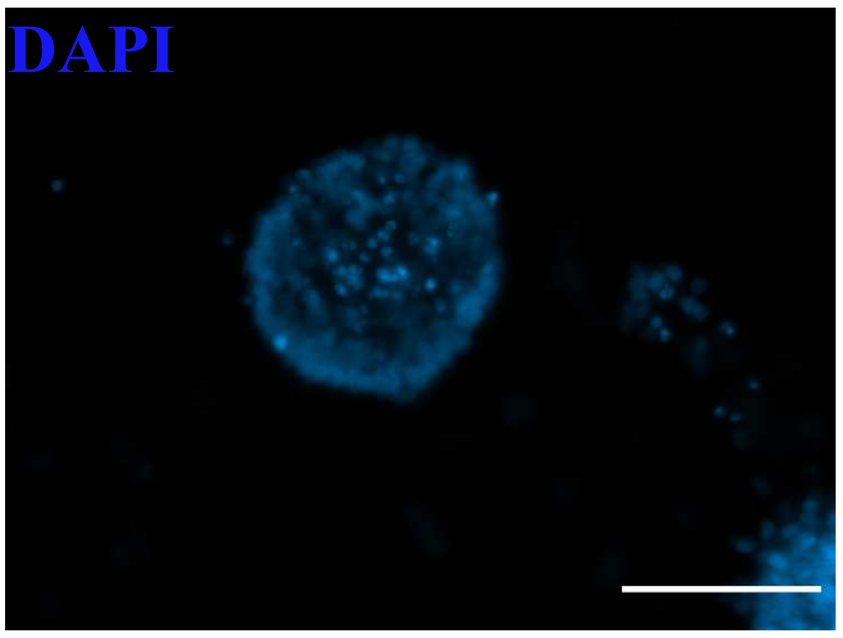
DAPI

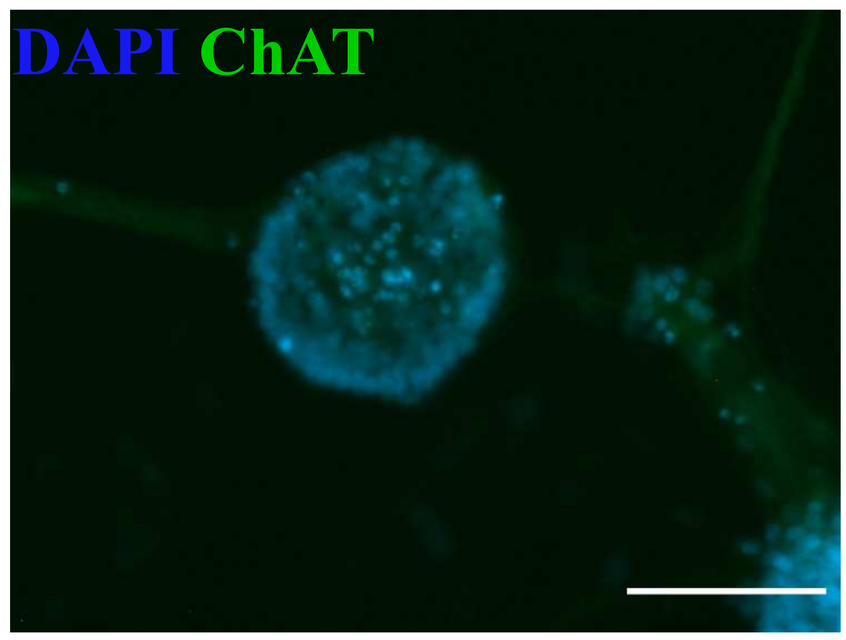
DAPI ChAT

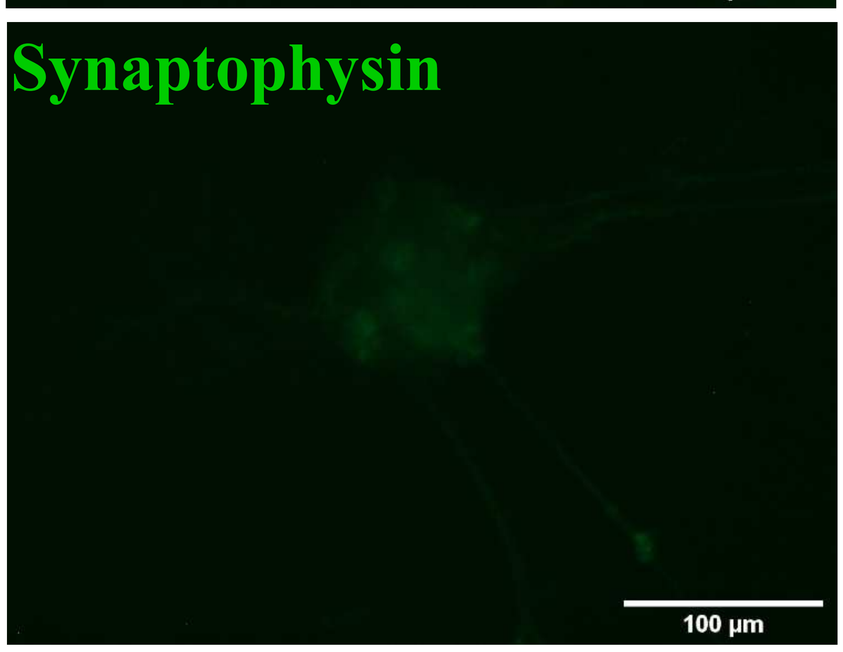
Synaptophysin
100 µm

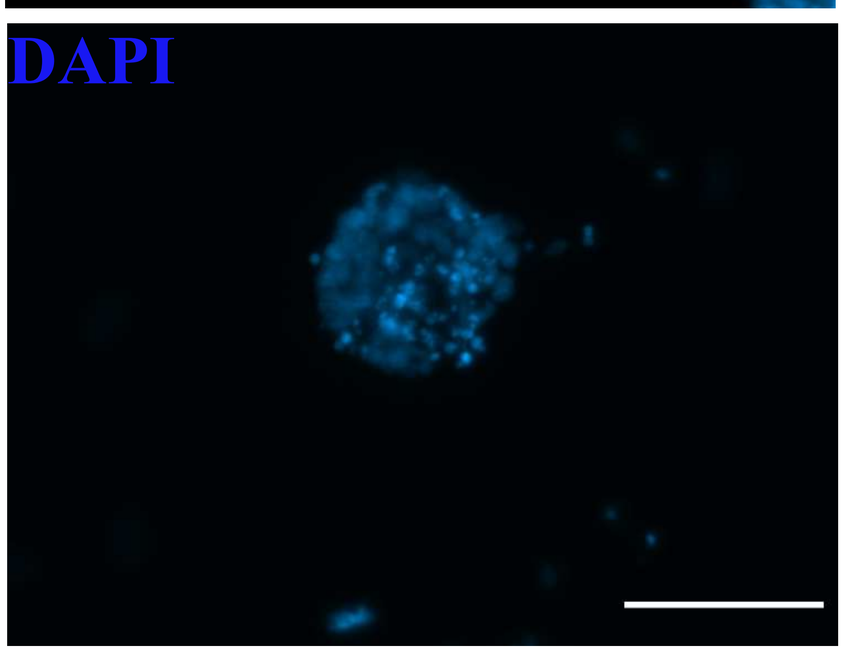
DAPI

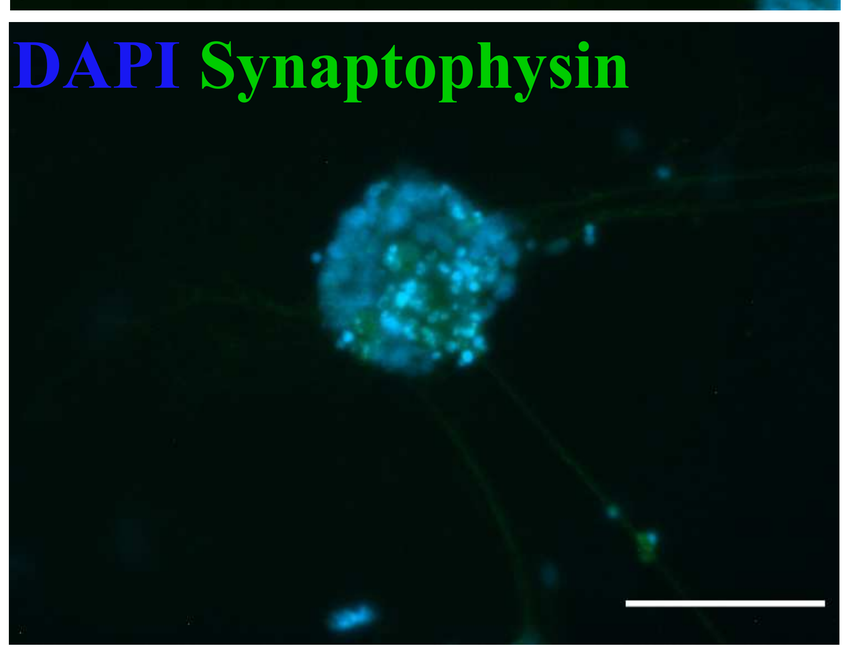
DAPI Synaptophysin

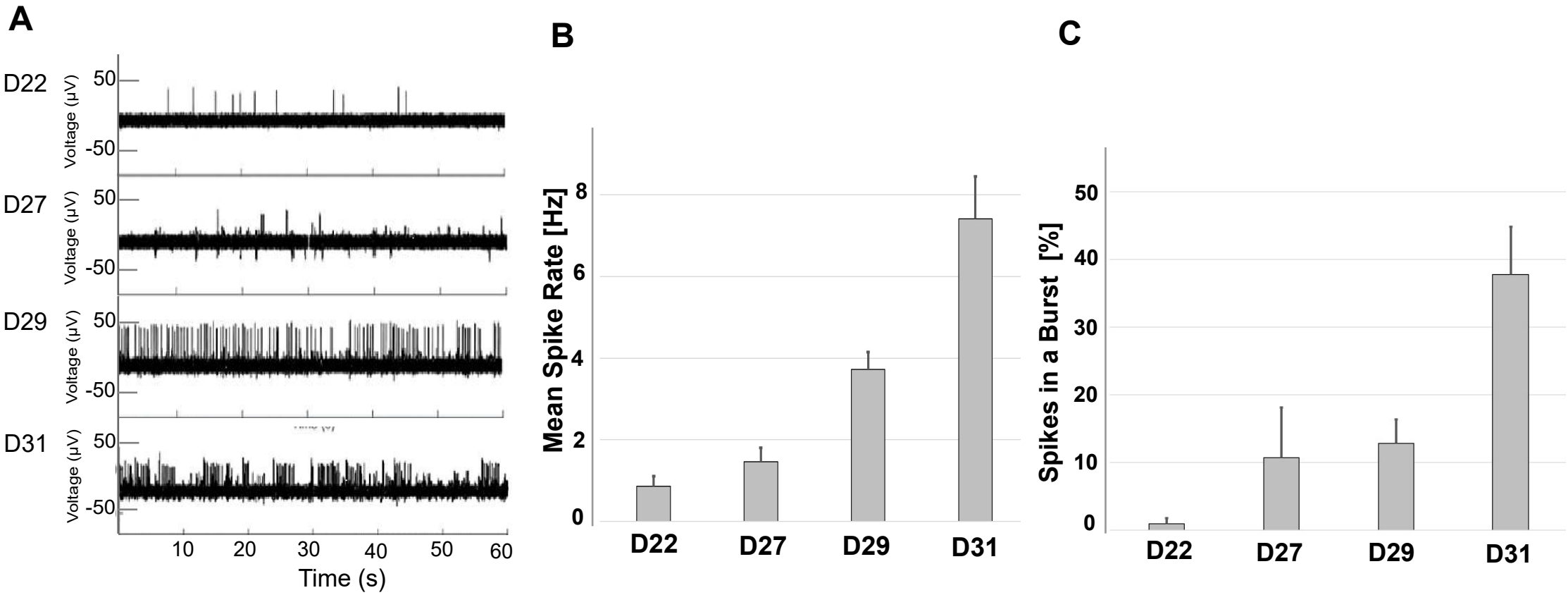
A
D22
D27
D29
D31
Voltage (μV)
50
-50
10
20
30
40
50
60
Time (s)
B
Mean Spike Rate [Hz]
0
2
4
6
8
D22
D27
D29
D31
C
Spikes in a Burst [%]
0
10
20
30
40
50
D22
D27
D29
D31

**Figure 2**

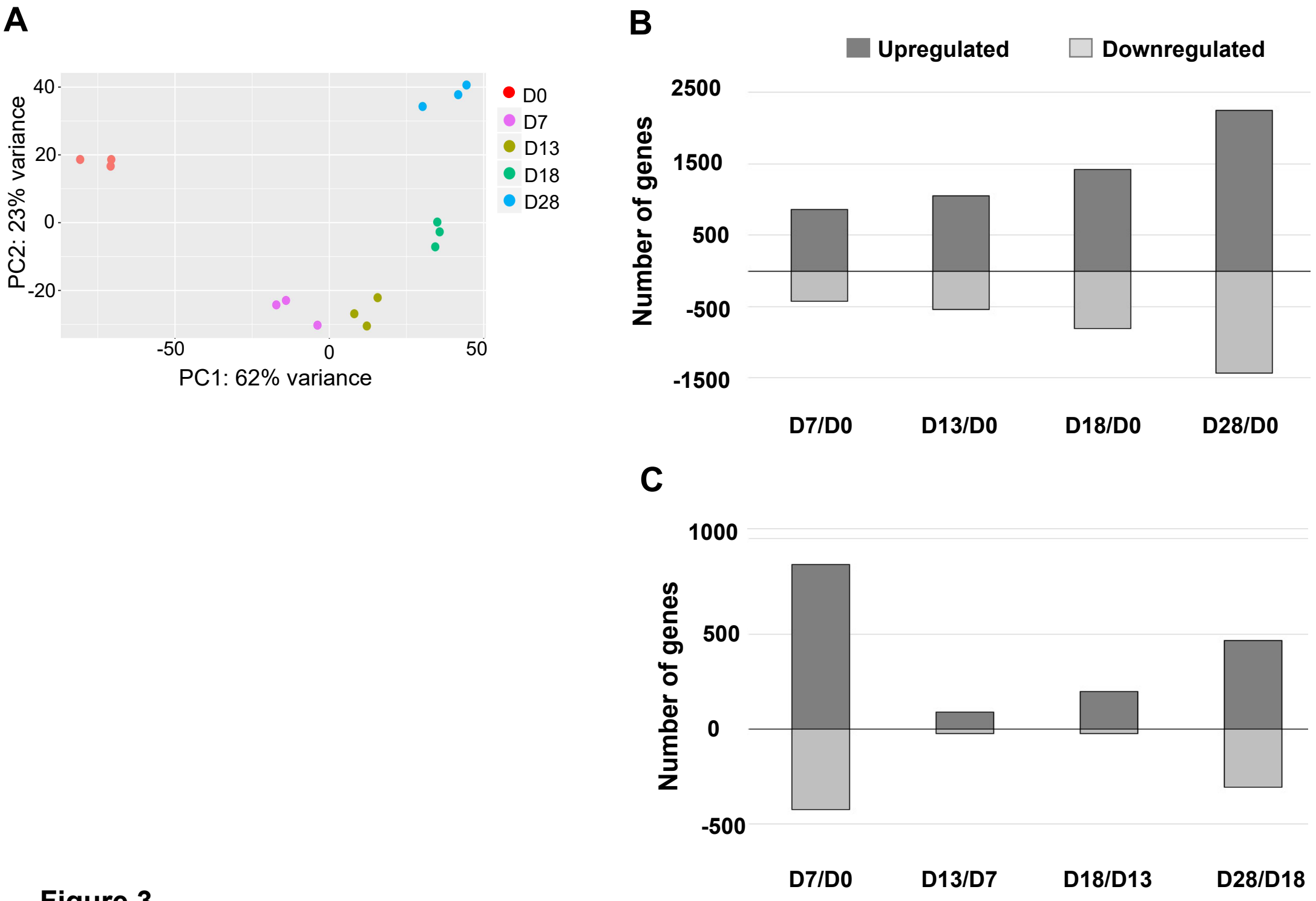
A
40
20
0
-20
PC2: 23% variance
-50
0
50
PC1: 62% variance
D0
D7
D13
D18
D28
B
Upregulated
Downregulated
2500
1500
500
-500
-1500
Number of genes
D7/D0
D13/D0
D18/D0
D28/D0
C
1000
500
0
-500
Number of genes
D7/D0
D13/D7
D18/D13
D28/D18

**Figure 3**

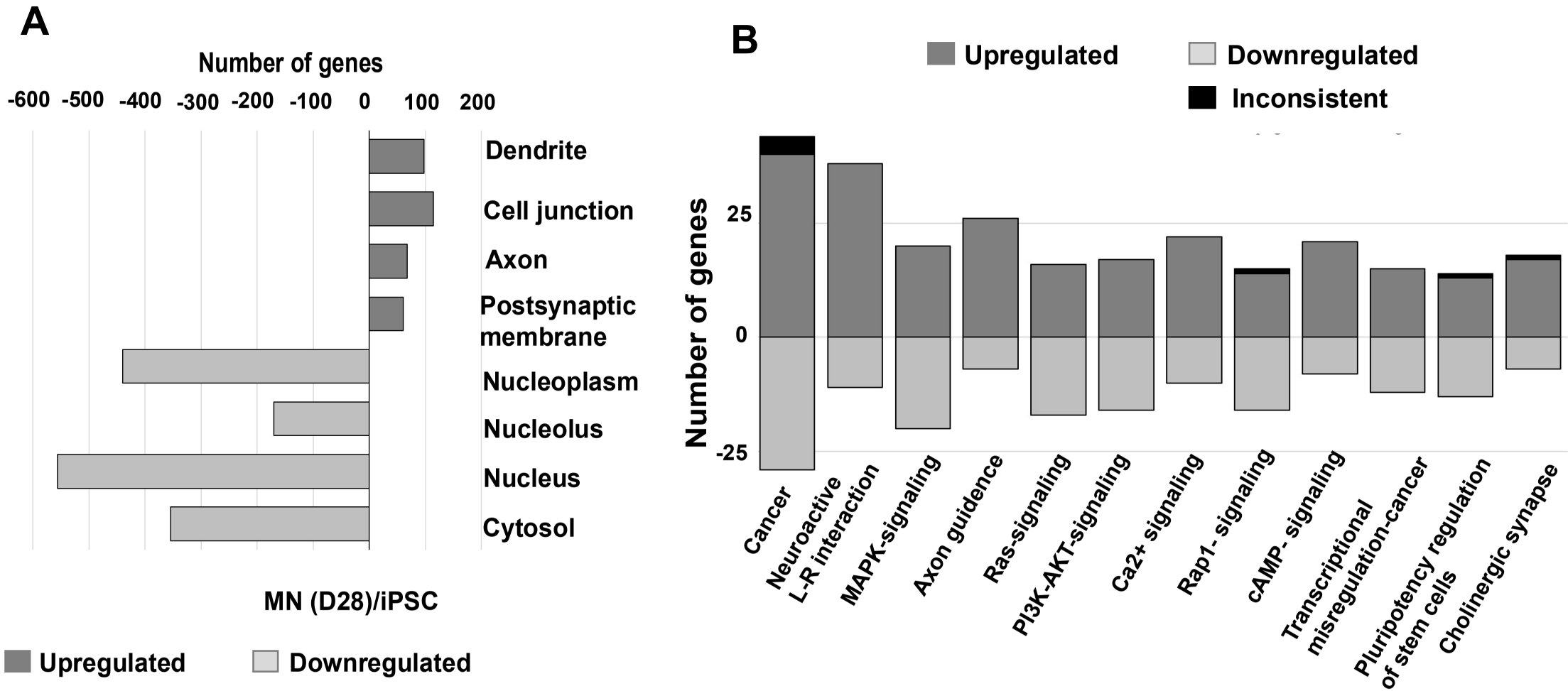
A
Number of genes
-600 -500 -400 -300 -200 -100 0 100 200
Dendrite
Cell junction
Axon
Postsynaptic membrane
Nucleoplasm
Nucleolus
Nucleus
Cytosol
MN (D28)/iPSC
Upregulated
Downregulated
B
Upregulated
Downregulated
Inconsistent
Number of genes
25
0
-25
Cancer
Neuroactive L-R interaction
MAPK-signaling
Axon guidence
Ras-signaling
PI3K-AKT-signaling
Ca2+ signaling
Rap1- signaling
cAMP- signaling
Transcriptional misregulation-cancer
Pluripotency regulation of stem cells
Cholinergic synapse

Figure 4

Figure 5

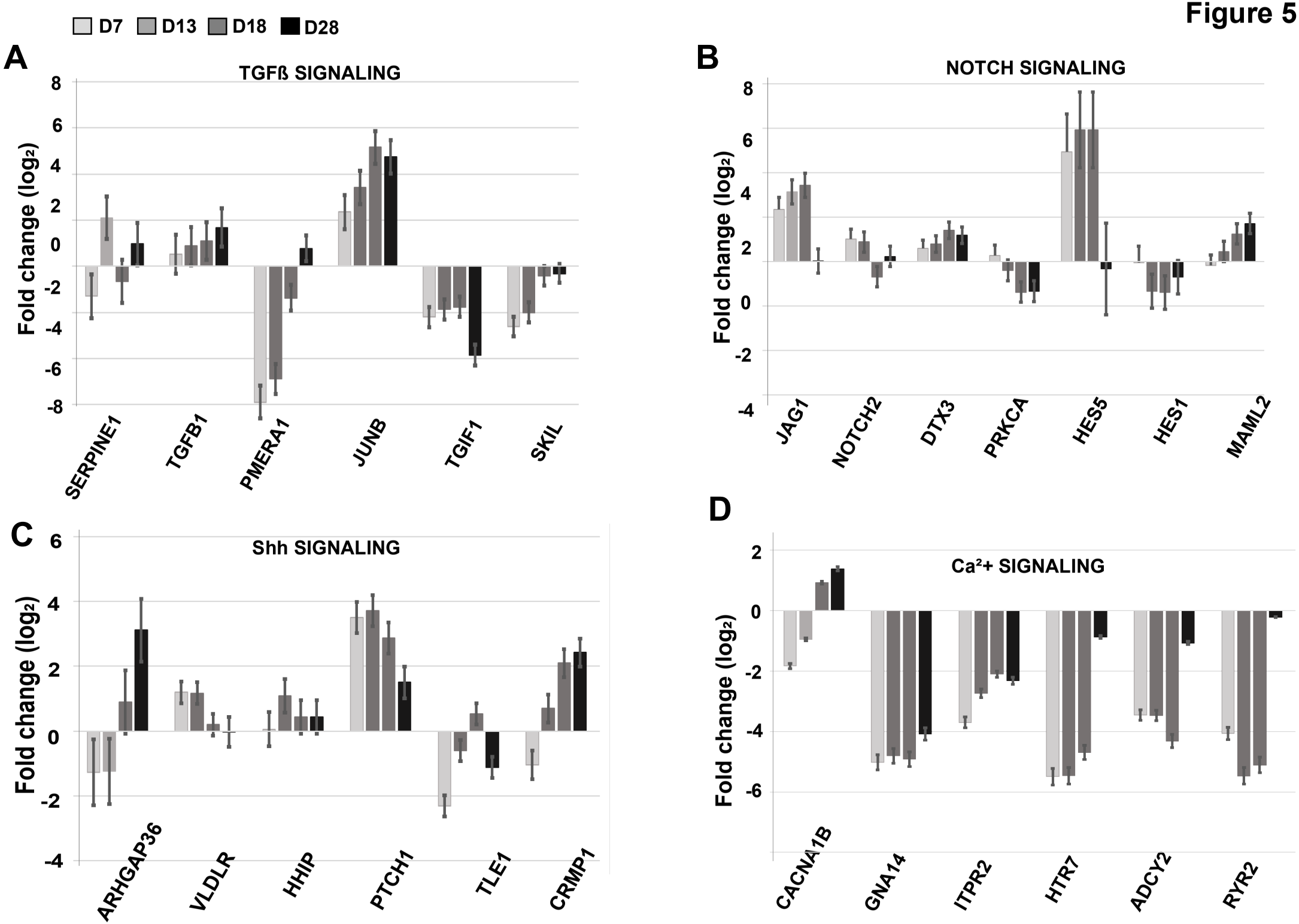
D7
D13
D18
D28
A
TGFß SIGNALING
Fold change (log2)
8
6
4
2
0
-2
-4
-6
-8
SERPINE1
TGFB1
PMERA1
JUNB
TGIF1
SKIL
B
NOTCH SIGNALING
Fold change (log2)
8
6
4
2
0
-2
-4
JAG1
NOTCH2
DTX3
PRKCA
HES5
HES1
MAML2
C
Shh SIGNALING
Fold change (log2)
6
4
2
0
-2
-4
ARHGAP36
VLDLR
HHIP
PTCH1
TLE1
CRMP1
D
Ca2+ SIGNALING
Fold change (log2)
2
0
-2
-4
-6
CACNA1B
GNA14
ITPR2
HTR7
ADCY2
RYR2

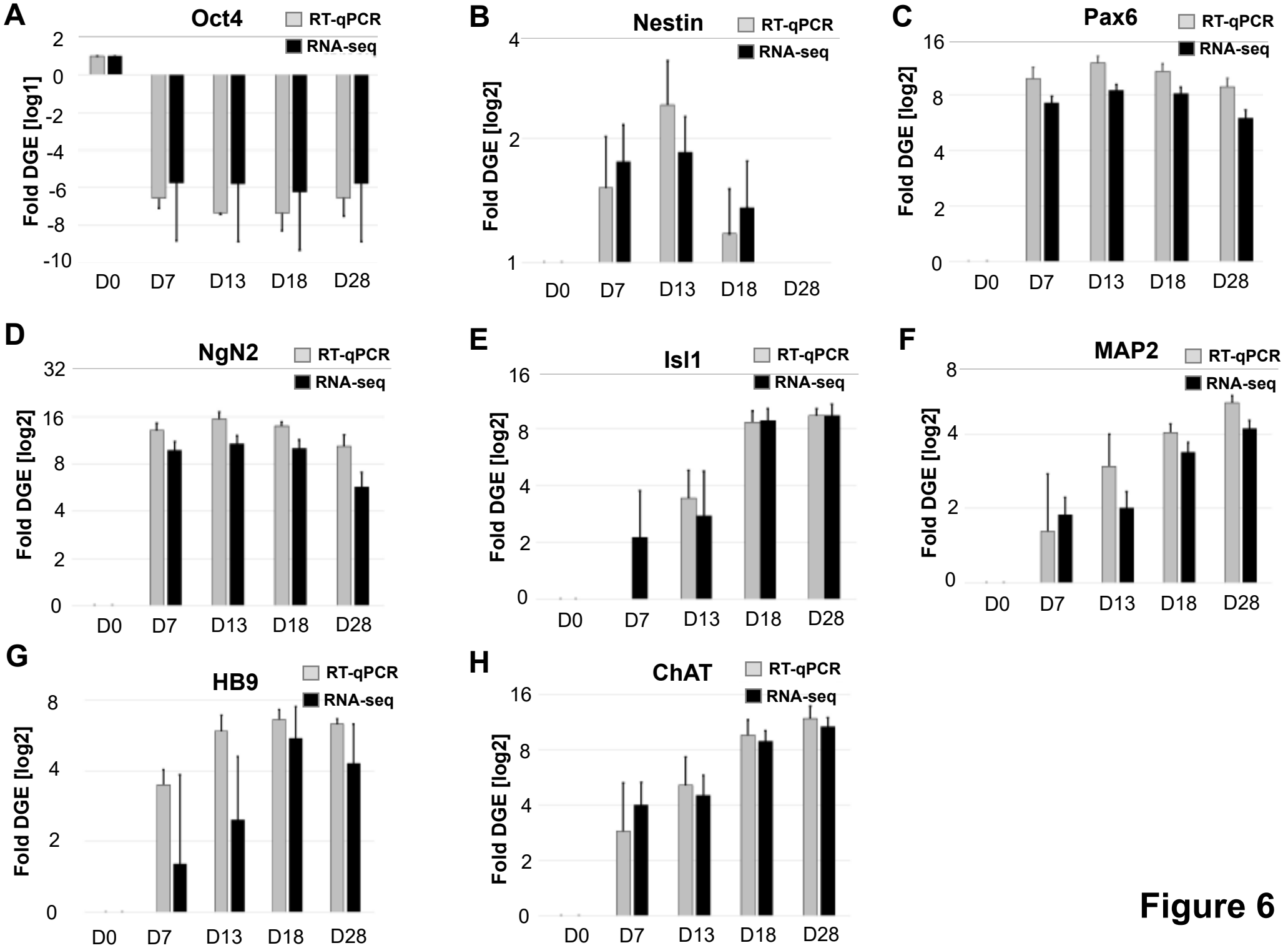
A
Oct4
RT-qPCR
RNA-seq
Fold DGE [log1]
2
0
-2
-4
-6
-8
-10
D0
D7
D13
D18
D28
B
Nestin
RT-qPCR
RNA-seq
Fold DGE [log2]
4
2
1
D0
D7
D13
D18
D28
C
Pax6
RT-qPCR
RNA-seq
Fold DGE [log2]
16
8
4
2
0
D0
D7
D13
D18
D28
D
NgN2
RT-qPCR
RNA-seq
Fold DGE [log2]
32
16
8
4
2
0
D0
D7
D13
D18
D28
E
Isl1
RT-qPCR
RNA-seq
Fold DGE [log2]
16
8
4
2
0
D0
D7
D13
D18
D28
F
MAP2
RT-qPCR
RNA-seq
Fold DGE [log2]
8
4
2
0
D0
D7
D13
D18
D28
G
HB9
RT-qPCR
RNA-seq
Fold DGE [log2]
8
4
2
0
D0
D7
D13
D18
D28
H
ChAT
RT-qPCR
RNA-seq
Fold DGE [log2]
16
8
4
2
0
D0
D7
D13
D18
D28

**Figure 6**

# Figures

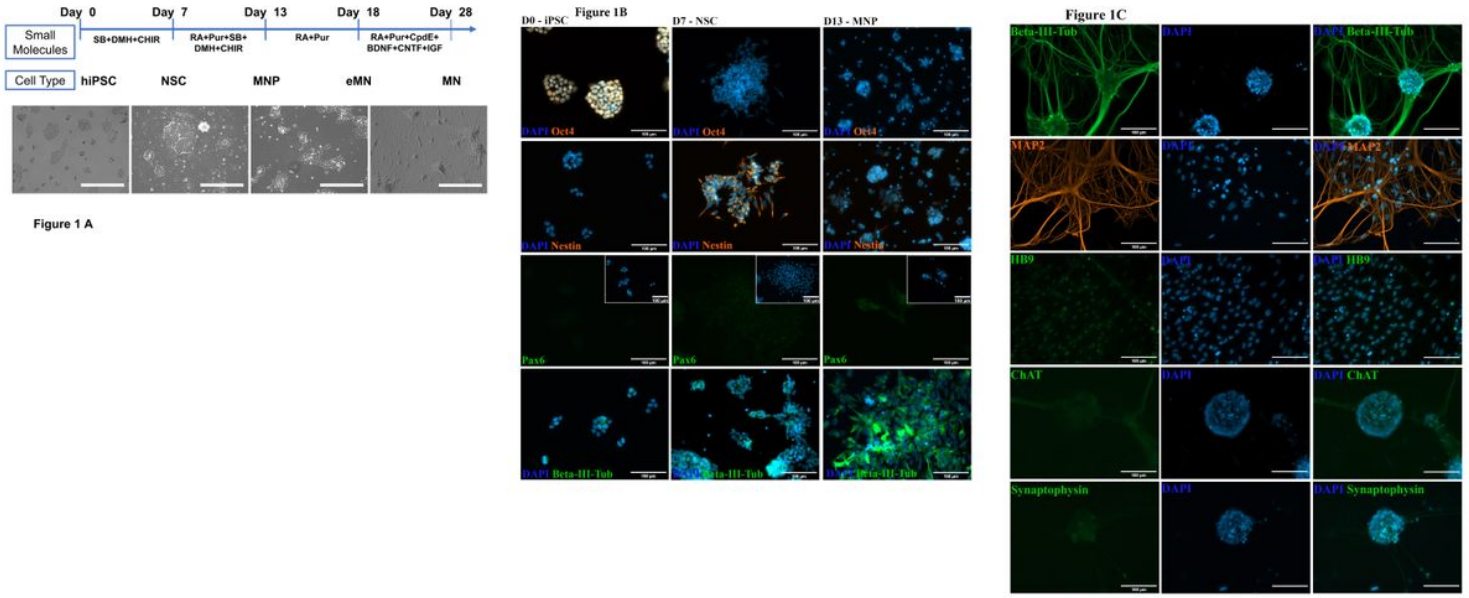


## Figure 1

Differentiation of WTC-11 induced pluripotent stem cells (iPSC) into motor neurons (MN). (A) Schematic diagram of the overall experimental design. Shown are the small molecule stimuli for each developmental stage and the corresponding morphological changes in the course of iPSC conversion into MN. The scale bar for the phase contrast images is 400 µm; (B) Representative immunofluorescence images of key pluripotency (Oct4) and pan-neuronal (Nestin, Pax6, and β-III tubulin) biomarkers indicated at efficient iPSC differentiation into neuronal stem cells (NSC) at day 7th post-induction (accumulation of Nestin is shown in orange). Upregulation of Pax6 and β-III tubulin (shown in green) at day 13 of iPSC induction marked the formation of motor neuron progenitor (MNP) cells. (C) Immunostaining of neuronal structural proteins (beta-III-tubulin in green, MAP2 in orange), motor neuron specific markers (HB9 and ChAT in green), and synaptic vesicles protein (Synaptophysin in green) showed a pure population of mature MN at day 28 post-stimulation of iPSC. Scale bar: 100 µm.

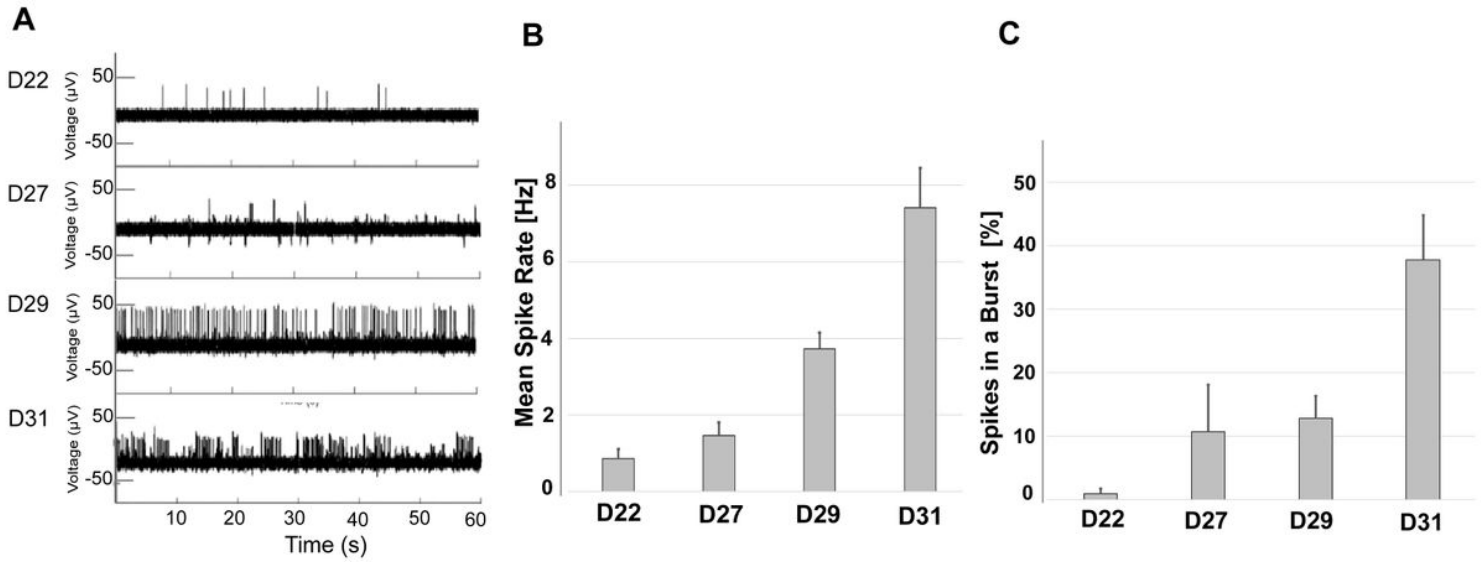


**Figure 2**

## Figure 2

Electrophysiological analysis of (MNs). (A) Time-dependent increase of spontaneous action potential (AP) spikes generated by MNs and recorded from a representative electrode (one of 144) on a multi-electrode (MEA) chip. MN were plated on the MEA chip at 18 days post chemical induction of iPSC (D18) and electrophysiological activity was recorded at the indicated time points of MN maturation (D22-D31) for 1 min. The frequency of AP spikes (B) and the percentage of spikes in the burst (C) dramatically increased within the neuronal networks over time. Shown are the mean and standard error from 12 electrodes at each sampling day post iPSC induction.

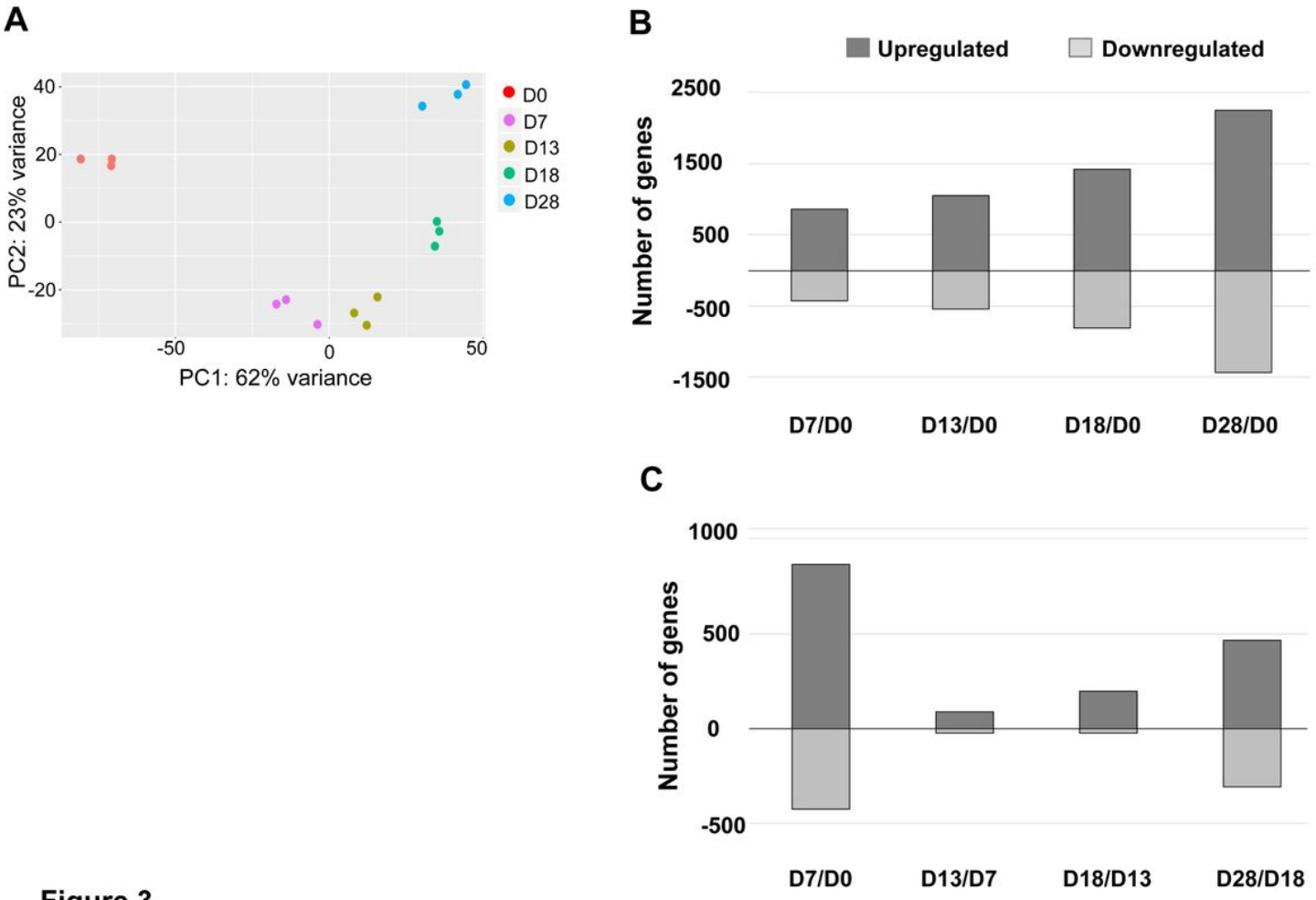


Figure 3

## Figure 3

Transcriptome analysis of cellular responses to MN maturation. (A) Principal component analysis of all samples, n=3; (B) Histogram of differentially expressed genes (DEGs) (adjusted $p < 0.0002$, fold change > 3) among D7 - D28 samples in the pairwise comparison with D0; (C) Histogram of DEGs in pairwise comparisons between adjacent timepoints (D0-D7, D7- D13, D13-18, D18-28).

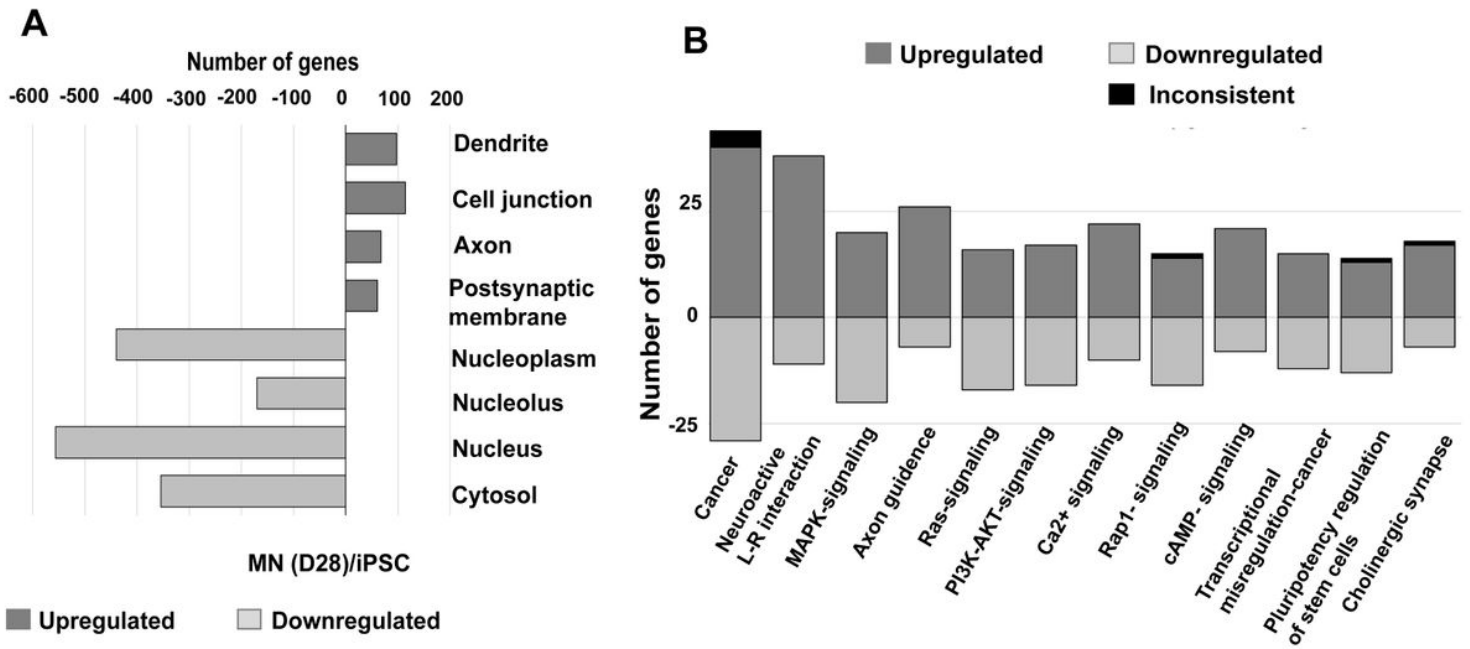


**Figure 4**

## Figure 4

Bioinformatics analysis of transcriptomic data. (A) Gene ontology (GO) analysis of iPSCs and MNs as determined by the NCBI Database for Annotation, Visualization and Integrated Discovery (DAVID). The top four significant GO terms of upregulated and downregulated genes are listed, ranked by p-value, when comparing D0 iPSCs and D28 MNs. (B) OPaver analysis of 12 KEGG pathways ranked by the number of DEG during the chemical reprogramming of iPSCs into MNs: Pathways in cancer; Neuroactive ligand-receptor interaction; MAPK-signaling pathway; Axon guidance; Ras signaling pathway; PI3K-Akt signaling pathway; Calcium signaling pathway; Rap1 signaling pathway; cAMP signaling pathway; Transcriptional mis regulation in cancer; Singling pathways regulating pluripotency of stem cells; and Cholinergic synapse.

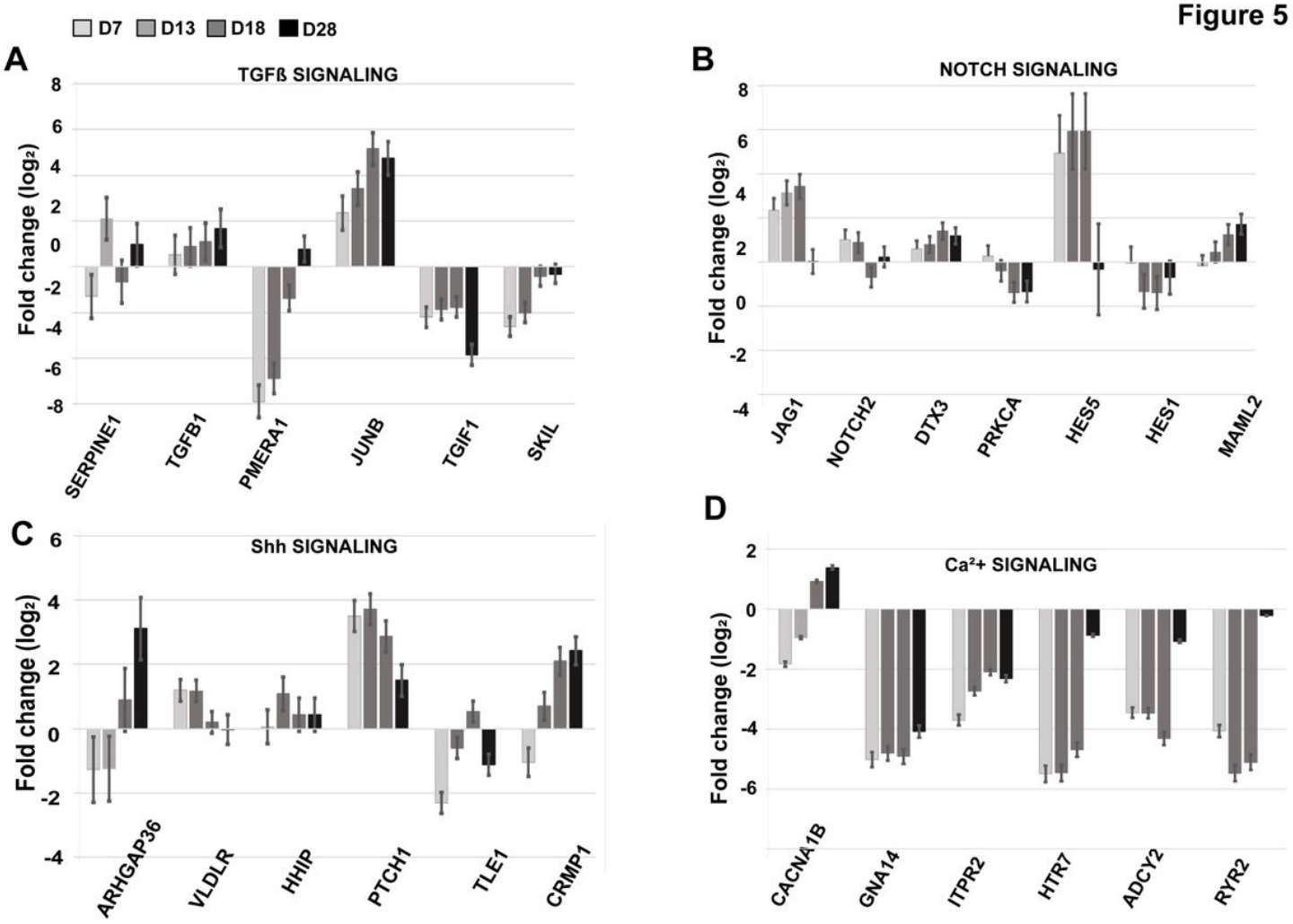


## Figure 5

Differential gene expression in key signaling pathways shaping MN differentiation. Gene transcript levels were determined by global RNA-seq analysis of (A) TGFβ, (B) Notch, and (C) Sonic Hedgehog (Shh) pathways. Fold change was calculated relative to RNA reads in iPSC (D0). The statistics (average value and standard error) were derived from three independent biological replicas with $p<0.001$ determined by R-statistical analysis package.

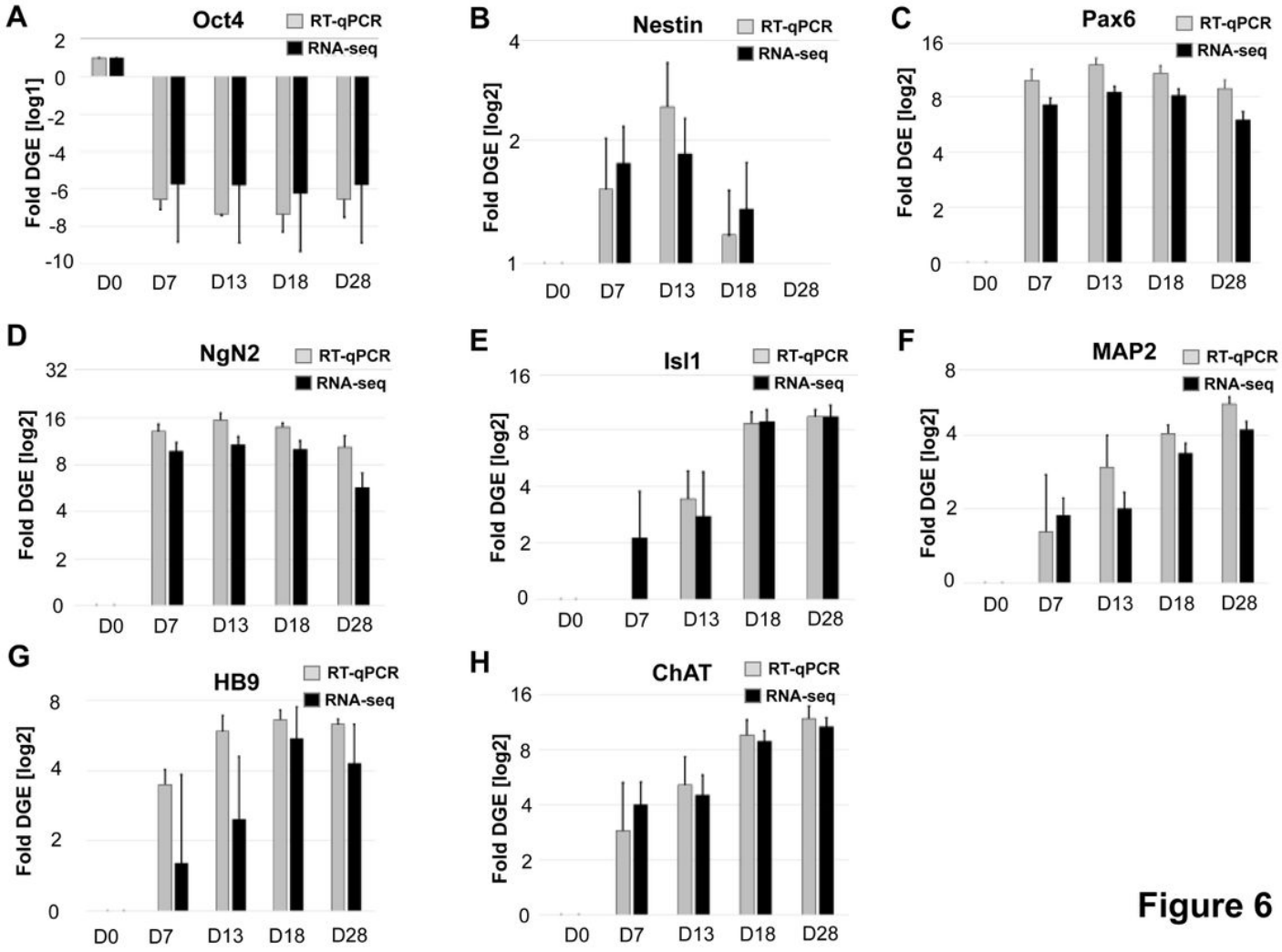


**Figure 6**

Comparative analysis of differential gene expression of key tissue development markers by RT-qPCR (gray) and RNA-seq (black). Pluripotency and NSC markers validated include (A) Oct4, transcription factor that maintains self-renewal and pluripotency; (B) Nestin, a filament protein marker of neural stem cells; (C) Pax6, a transcription factor that drives neurogenesis; and (D) NgN2, a neuronal-specific transcription factor. Motor neuron specification markers validated include (E) Isl1, a transcription factor required for motor neuron generation; (F) Map2, a neuron specific cytoskeletal protein; (G) HB9, an early marker of cholinergic neurons; and (H) ChAT, an enzyme required for acetylcholine synthesis. Shown are the averages and standard error from three independent biological replicas from the iPSC to MN differentiation trajectory. The RNA-Seq transcripts were normalized to the total read per analyzed sample (in FPKM: fragments per kilobase per million mapped fragments) and the transcript levels determined by RT-qPCR were normalized to GAPDH as the endogenous sample control. Fold change was calculated for each developmental stage relative to transcript levels in iPSC (D0). Statistical significance ($p < 1.5e-6$) was determined with Student t-test.

# Supplementary Files

This is a list of supplementary files associated with this preprint. Click to download.

- D0D13DEGsignificant.xlsx
- D0D18DEGsignificant.xlsx
- D0D28DEGsignificant.xlsx
- D0D7DEGsignificant.xlsx
- D13D18DEGsignificant.xlsx
- D13D28DEGsignificant.xlsx
- D18D28DEGsignificant.xlsx
- D7D13DEGsignificant.xlsx
- D7D18DEGsignificant.xlsx
- D7D28DEGsignificant.xlsx